

BRL R 1514

AD719235

# BRL

AD

REPORT NO. 1514

THE INFLUENCE OF HELICAL SERRATIONS AND BULLET ENGRAVING  
ON THE AERODYNAMIC AND STABILITY PROPERTIES  
OF A BODY OF REVOLUTION WITH SPIN

by

M. A. Sylvester  
W. F. Braun

November 1970

DDC  
RECEIVED  
MAR 2 1971  
REGULATED  
B

This document has been approved for public release and sale;  
its distribution is unlimited.

U.S. ARMY ABERDFEN RESEARCH AND DEVELOPMENT CENTER  
BALLISTIC RESEARCH LABORATORIES  
ABERDEEN PROVING GROUND, MARYLAND

Reproduced by  
NATIONAL TECHNICAL  
INFORMATION SERVICE  
Springfield, Va. 22151

53

BALLISTIC RESEARCH LABORATORIES

REPORT NO. 1514

NOVEMBER 1970

THE INFLUENCE OF HELICAL SERRATIONS AND BULLET ENGRAVING  
ON THE AERODYNAMIC AND STABILITY PROPERTIES  
OF A BODY OF REVOLUTION WITH SPIN

M. A. Sylvester  
W. F. Braun

Exterior Ballistics Laboratory

This document has been approved for public release and sale;  
its distribution is unlimited.

This project was sponsored by U.S. Army Small Arms Svstems Agency  
under RDT&E Project No. 1W562604A607

ABERDEEN PROVING GROUND, MARYLAND

BALLISTIC RESEARCH LABORATORIES

REPORT NO. 1514

MASylvester/WFBraun/lca  
Aberdeen Proving Ground, Md.  
November 1970

THE INFLUENCE OF HELICAL SERRATIONS AND BULLET ENGRAVING  
ON THE AERODYNAMIC AND STABILITY PROPERTIES  
OF A BODY OF REVOLUTION WITH SPIN

ABSTRACT

Discrepancies in the predicted and observed stability behavior of bullets sometimes occur at longer ranges. Experiments in the BRL supersonic wind tunnel and range suggest that this behavior may be due to subtle aerodynamic effects of the helical engraving. The wind tunnel tests were made at supersonic Mach numbers on spinning models with accentuated helical serrations. The tests covered a range of angle of attack, Reynolds number and mismatch between the spin of the model and the twist of the serrations. The serrated model test results show yaw force and moment characteristics basically different than the Magnus results for a similar but nonserrated model. These serrated results indicate yaw forces and moments at higher angles of attack which are finite even at zero spin and which then decrease and reverse sign as the spin increases. At lower angles of attack the yaw data are extremely sensitive to the Reynolds number and the boundary layer condition and may be highly non-linear with both angle of attack and spin mismatch.

The range data were obtained on both standard ammunition and models. For the roll damping moment a formulation is proposed and the roll moment coefficients are established for one particular model. The effects on the static moments are shown to be negligible. The Magnus and damping moments are changed, indicating a requirement for a formulation not dependent on mirror symmetry. The exponential damping coefficients show an increase in the fast mode damping with underspin and indicate strong nonlinearities in the slow mode.

## TABLE OF CONTENTS

	Page
ABSTRACT . . . . .	3
LIST OF ILLUSTRATIONS . . . . .	7
LIST OF SYMBOLS . . . . .	9
1. INTRODUCTION . . . . .	11
2. WIND TUNNEL TESTS AND RESULTS . . . . .	13
2.1 Test Facility . . . . .	13
2.2 Models and Equipment . . . . .	15
2.3 Test Technique . . . . .	16
2.4 Data Reduction . . . . .	17
2.5 Results and Discussion . . . . .	18
2.5.1 General . . . . .	18
2.5.2 Comparison of Serrated and Nonserrated Model Results . . . . .	18
2.5.3 Correlation for Different Amounts of Serration Twist . . . . .	22
2.5.4 Additional Serrated A-N Spinner Yaw Data Characteristics . . . . .	25
3. FREE FLIGHT RANGE INVESTIGATION . . . . .	33
3.1 Test Facility and Routine Techniques . . . . .	33
3.2 Special Techniques for Spin Mismatch Measurements . . . . .	33
3.3 General Test Plan . . . . .	35
3.4 The Models . . . . .	36
3.5 Results . . . . .	36
3.5.1 Detection Phase Range Program . . . . .	36
3.5.2 The Static Aerodynamic Properties . . . . .	38
3.5.3 The Magnus and Damping Moments . . . . .	41
3.5.4 The Rolling Motion . . . . .	41
3.5.5 The Damping Coefficients . . . . .	46

TABLE OF CONTENTS (Continued)

	Page
4. CONCLUSIONS . . . . .	47
REFERENCES . . . . .	49
DISTRIBUTION LIST . . . . .	51

## LIST OF ILLUSTRATIONS

Figure	Page
1. Wind Tunnel Models . . . . .	14
2. Serrated A-N Spinner Model Installed in Wind Tunnel . . . . .	16
3. Comparison of Typical Serrated and Nonserrated Results for the Cone-Cylinder Models: $M = 1.5$ , $Re_{\rho} = 5.1 \times 10^6$ . . . . .	19
4. Comparison of Serrated and Nonserrated Results for the A-N Spinner: $M = 2.0$ , $Re_{\rho} = 4.0 \times 10^6$ . . . . .	23
5. Comparison of Serrated Cone-Cylinder and A-N Spinner Data . . . . .	24
6. Serrated A-N Spinner Yaw Force Coefficient Data Trends for Several Angle of Attack Ranges at a Reynolds Number of $4 \times 10^6$ . . . . .	26
7. Serrated A-N Spinner Yaw Moment Coefficient Data Trends for Several Angle of Attack Ranges at a Reynolds Number of $4 \times 10^6$ (Moments Referred to Model Base) . . . . .	26
8. Serrated A-N Spinner Yaw Force Coefficient Data Trends for Several Angle of Attack Ranges at a Reynolds Number of $2 \times 10^6$ . . . . .	29
9. Serrated A-N Spinner Yaw Moment Coefficient Data Trends for Several Angle of Attack Ranges at a Reynolds Number of $2 \times 10^6$ (Moments Referred to Model Base) . . . . .	29
10. Serrated A-N Spinner Yaw Force and Moment Data for Positive and Negative Angles of Attack at a Reynolds Number of $2 \times 10^6$ (Moments Referred to Model Base) . . . . .	31
11. Effect of Reynolds Number on the Yaw Force and Moment Characteristics of the Serrated A-N Spinner: $\alpha \approx 1.1$ Degree (Moments Referred to Model Base) . . . . .	32
12. Effect of Boundary-Layer Trip on the Yaw Force and Moment Characteristics of the Serrated A-N Spinner at a Reynolds Number of $2 \times 10^6$ : $\alpha = 1.0$ Degree (Moments Referred to Model Base) . . . . .	32
13. Spark Photograph of Pre-engraved A-N Spinner Rocket Model, Mach 1.85, Underspin Flight . . . . .	34
14. Range Test Models . . . . .	37

LIST OF ILLUSTRATIONS (Continued)

Figure	Page
15. Magnus Moment Coefficient, Caliber .30 Ball M2, Effect of Underspin . . . . .	39
16. Damping Moment Coefficient, Caliber .30 Ball M2, Effect of Underspin . . . . .	39
17. Static Coefficients Vs. Spin Mismatch Ratio, Sarp 1B Models, Mach 1.42 . . . . .	40
18. Static Moment Coefficient Vs. Spin . . . . .	40
19. The Magnus Moment Coefficient, Sarp 1B Model, Mach 1.42 . .	42
20. The Damping Moment Coefficients, Sarp 1B Model, Mach 1.42 .	42
21. Roll Damping, Free Spinning Serrated Model . . . . .	45
22. Rolling Moments, Caliber .30 Sarp 1B Model, Mach 1.42 . . .	45
23. The Exponential Damping Coefficients, Sarp 1B Models . . . .	46

## LIST OF SYMBOLS

$d$	model diameter
$k_a$	axial radius of gyration
$m$	mass of missile
$p$	model rotational speed
$\frac{pd}{V}$	nondimensional spin rate
$\frac{pd}{V} = 2 \tan \delta_g$	matchspin
$\frac{pd}{V} > 2 \tan \delta_g$	overspin
$\frac{pd}{V} < 2 \tan \delta_g$	underspin
$C_n$	yaw moment coefficient
$C_D$	drag coefficient
$C_Y$	yaw force coefficient
$C_{M_\alpha}$	$\frac{\text{Static Moment}}{(1/2) \rho V^2 S d \alpha_t}$ Positive coefficient: moment increases angle of attack $\alpha_t$
$C_{M_{p_\alpha}}$	$\frac{\text{Magnus Moment}}{(1/2) \rho V^2 S d \frac{pd}{V} \alpha_t}$ Positive coefficient: moment rotates missile nose in direction of spin
$C_{M_q} + C_{M_{\dot{\alpha}}}$	$\frac{\text{Damping Moment}}{(1/2) V^2 S d \frac{q_t d}{V}}$ Positive coefficient: moment increases angular velocity
$C_{N_\alpha}$	$\frac{\text{Normal Force}}{(1/2) \rho V^2 S \alpha_t}$ Positive coefficient: force acts in the direction of the angle of attack $\alpha_t$
$C_{L_p}$	$\frac{\text{Roll Damping Moment}}{(1/2) \rho V^2 S d \left(\frac{pd}{V}\right)}$ Negative coefficient: moment opposes rolling moment

LIST OF SYMBOLS (Continued)

$C_{l\delta}$	<u>Roll Moment Due to Mismatch</u> $(1/2) \rho V^2 S d [\tan \delta_g - (\frac{pd}{V})]$	Negative coefficient: moment opposes rolling moment for the overspin condition
$I_x$	axial moment of inertia	
M	Mach number	
$Re_l$	Reynolds number based on model length and free stream conditions	
S	$\pi d^2/4$	
V	free stream velocity; velocity of missile	
$\alpha$	angle of attack	
$\alpha_t$	$(\alpha^2 + \beta^2)^{1/2}$ , $\sin^{-1} \delta$ , total angle of attack	
$\alpha_t$	arc sin $\sqrt{\delta^2}$	
$\delta_g$	serration angle or bullet-engraving angle (angle between the projectile longitudinal axis and the developed helix)	
$\lambda_{F,S}$	fast and slow yaw damping rates	
<u>Subscripts</u>		
o	initial conditions	
R	range values	

## 1. INTRODUCTION

The analysis of the motion of gyroscopically-stabilized and fin-stabilized projectiles is frequently based on the linearized equations of motion of symmetric missiles<sup>1\*</sup>. This is particularly true for preliminary analyses even when the required assumptions are obviously not entirely valid. The three basic areas in which the usual formulations may differ from the actual projectile case are: (1) large yaw, where the small yaw assumptions break down; (2) aerodynamic nonlinearities, even at small yaw; and (3) lack of rotational and mirror symmetry. All of these areas have, at times, had to be considered, especially where extreme violations of the usual assumptions were apparent.

Cases involving deviations from mirror symmetry have been considered and reported<sup>2,3</sup> but primarily for the more prominent case of finned projectiles. As far as is known, the influence of the less dramatic lack of mirror symmetry associated with the grooving or firing bands of the spin-stabilized projectile has rarely been considered.

In the case of the finned projectiles, important effects can develop within several periods of yaw because of the high-lift-producing fins. In contrast, the rotating band and engraving on spin-stabilized shell and bullets are much less pronounced and their effects may be mostly shrouded by the viscous boundary layer. These effects would, therefore, tend to be less obvious and probably become apparent only after many periods of yaw, or well down range. While this would appear to suggest the category of long range artillery as being more susceptible, bullets can also have relatively long ranges in relation to their size or in terms of calibers of travel. In fact, the bullet may be considerably more sensitive to mirror asymmetry effects because the engraving is usually more extensive than that associated with the firing band of the larger shell. This conjecture would appear to be further strengthened by the fact that no detectable effects have been observed for large shell whereas some discrepancies have been noted for bullets.

---

\* References are listed on page 49.

The unpredicted stability behavior of bullets at longer ranges has stimulated several experimental studies to determine the cause. One investigation<sup>4</sup> was concerned with the possible contributions of bullet deformations but the effects, although measurable, did not explain the observed discrepancies. Another and continuing study is the subject of the present paper and is concerned primarily with the effects of helical serrations and bullet engraving on the aerodynamic and stability characteristics of bodies of revolution with spin. Several experimental investigations in this area of concern have been made or are planned in the wind tunnel and range, and some previously obtained data have been reviewed.

A condition of considerable significance in the discussion of the results of the tests and their interpretation involves the concept of matchspin and spin mismatch. Matchspin is defined as the condition where the nondimensional spin rate is equal to twice the tangent of the serration or engraving angle,  $pd/V = 2 \tan \delta_g$ . This, in effect, specifies the spin rate,  $p$ , at which air flow with velocity,  $V$ , would pass through the serrations without being deflected. For practically all bullets the axial deceleration is greater than the spin deceleration. At the gun muzzle the engraving caused by the twist of rifling of the gun matches the spin of the bullet. Down range, the velocity has decreased more than the spin, so that the spin rate is greater than twice the tangent of the engraving angle,  $pd/V > 2 \tan \delta_g$ . This condition is called overspin. In a normal test in the 300 ft. range facility, the overspin is not likely to be more than 10 percent. At long range the overspin may be as much as 100 percent. In some range tests, it is more convenient to decrease the spin after the bullet is fired. The spin rate is then less than twice the tangent of the engraving angle and this flight condition is called underspin,  $pd/V < 2 \tan \delta_g$ . In the wind tunnel, both overspin and underspin can be readily obtained so long as the matchspin condition does not exceed the maximum test capability. Underspin and overspin effects would be expected to be similar, although possibly of different sign.

The wind tunnel tests were made at supersonic Mach numbers on models with relatively deep helical serrations. The completely serrated cone-cylinder model was selected as an initial research vehicle but was later replaced by the more realistic A-N spinner with serrations on the cylindrical portion only. The twist of the serrations on the A-N spinner was also reduced in order to provide an overspin capability which was not available with the cone-cylinder model due to test limitations. Although this reduction in twist resulted in a model with considerably less than typical bullet twist, the provision of matchspin and overspin conditions was felt to be of overriding importance. The accentuated serrations were deemed desirable in these preliminary tests to assure that measurable, even though somewhat exaggerated, trends would be obtained. The tests covered ranges of angle of attack, Reynolds number and spin mismatch which included values typical of bullet conditions.

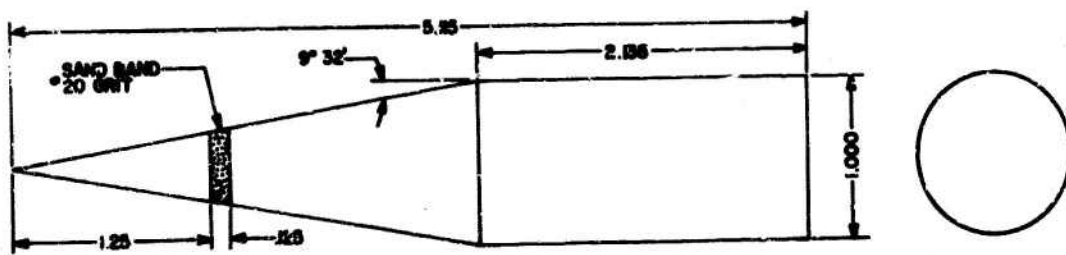
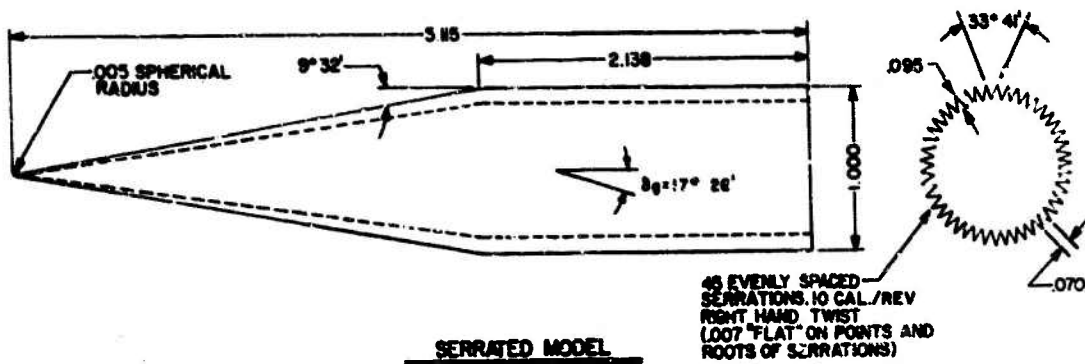
The initial range program had the sole objective of determining whether the mismatch condition could produce a detectable effect on a bullet and, if so, whether it was of a nature that could explain the observed discrepancies. This aeroballistic range program of necessity used actual ammunition, the caliber .30 M2 bullet, the 7.62mm M80 and the 5.56mm M193. This produced positive results and additional programs were added to define the pertinent variables and to obtain quantitative data for bullet shapes.

Since the lead core bullets are inconsistent aerodynamic test vehicles because of variations in flight shape and physical properties, the second range program used caliber .30 bronze bullet models. These were tested in the matchspin and underspin condition. Additional programs are in progress using a 5 caliber A-N spinner rocket shape engraved for the 20mm gun.

## 2. WIND TUNNEL TESTS AND RESULTS

### 2.1 Test Facility

The wind tunnel tests were conducted in the Ballistic Research Laboratories' Supersonic Wind Tunnel No. 1<sup>5</sup>. This tunnel is of the



ALL DIMENSIONS IN CALIBERS  
(CALIBER = 2000 INCHES)

**NON-SERRATED MODEL WITH SAND BAND**

**a. CONE-CYLINDER**

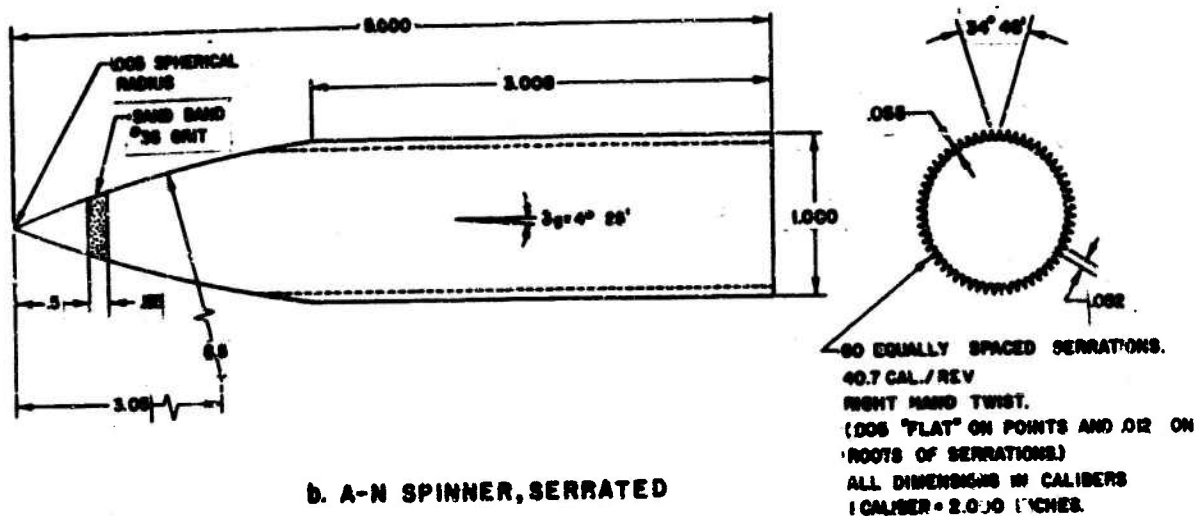


Figure 1. Wind Tunnel Models

continuous flow, variable density type and has a flexible nozzle for obtaining a range of Mach numbers from approximately 1.5 to 5.0. The test section size is 13 inches wide by 15 inches high and the flow quality (including flow inclination, Mach number variation and turbulence level) is very good. Therefore, this tunnel is particularly well suited for "Magnus-type" measurements since the relatively low-level forces and moments will not be obscured by undesirable tunnel conditions.

## 2.2 Models and Equipment

The models used in the wind tunnel tests are illustrated in Figure 1. The models all have a diameter of two inches (measured to the serration extremity) and are about 5 calibers in length. The cone-cylinder models have a cylindrical-section length of only about 2 calibers whereas, for the A-N spinner, this section is 3 calibers. The serrated cone-cylinder model has 45 evenly-spaced serrations with a right-hand twist of 10 calibers per turn ( $\delta_g = 17^\circ 26'$ ). The serrations cover the entire model surface and have a depth of 0.095 caliber on the cylindrical section and then taper out to zero at the nose. The 60 serrations of the A-N spinner, covering essentially only the cylindrical section, are about half as deep (0.055 caliber) and have considerably less twist (40.7 calibers per turn or  $\delta_g = 4^\circ 25'$ ).

The models were sting supported for the wind tunnel tests (Figure 2) and were mounted on a 4-component strain-gage balance which provided measurements of the forces and moments in the yaw and pitch planes. The models were attached to the balance through a ball bearing and sleeve arrangement which allowed the model to rotate. A locking device was provided to prevent the serrated models from rotating during the tunnel starting conditions and a nozzle-turbine combination was used to rotate the model in the clockwise direction (looking upstream). The rotational speed of the model was indicated by a coil-magnet pickup in the model and a thermocouple was used to monitor balance temperatures. The output signals from the balance, the rpm pickup and thermocouple were conditioned and recorded on X-Y plotters.

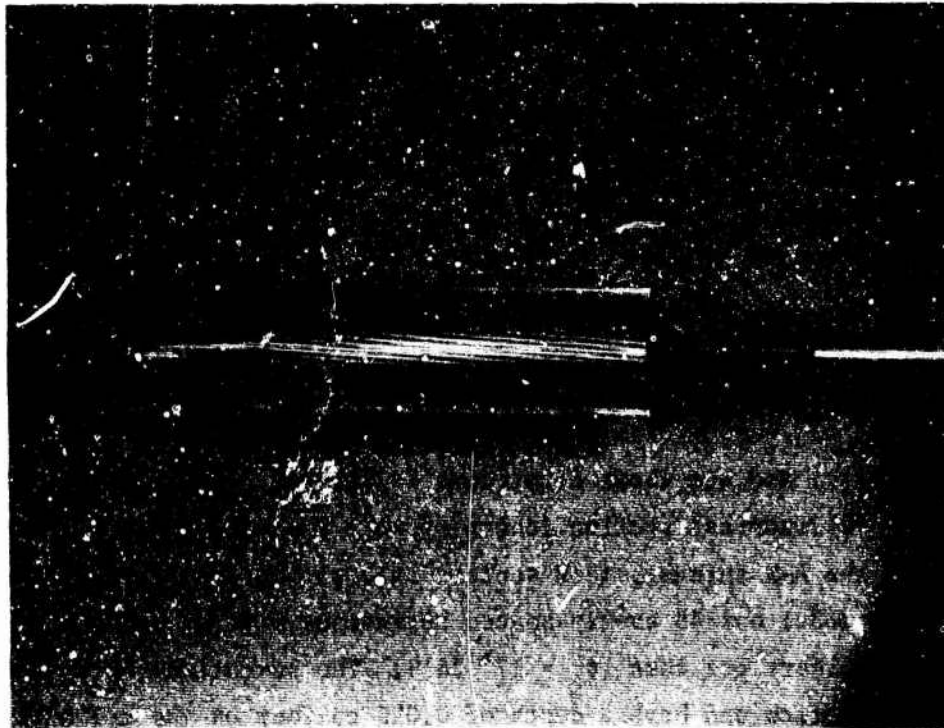


Figure 2. Serrated A-N Spinner Model Installed in Wind Tunnel

### 2.3 Test Technique

The testing procedure for the nonserrated model was to simply start the tunnel and then use the air turbine to spin the model up to the maximum rotational speed of about 40,000 revolutions per minute. The air to the turbine was then shut off and the pitch and yaw data were recorded as a function of rpm as the model coasted to a stop.

The test procedure for the serrated models was somewhat different due to the inherent tendency of these models to spin as the result of the air flow over the serrations. For these tests, the model was locked until the tunnel flow was established. It was then unlocked and data obtained as the model spun up to its experimental free-spin rate. The air turbine was then actuated and the model spun still higher until the maximum rotational speed was reached. Again data were obtained as the model spin rate decayed to its experimental free-spin value. By this method, data could be obtained both below and above the experimental

free-spin rate. Roll damping data could be obtained by recording the spin-up and spin decay as functions of time.

#### 2.4 Data Reduction

Although these tests on spinning models are similar to the usual Magnus type, the data obtained on the serrated models are basically different in some respects as will be shown later. Therefore, to avoid confusion, the wind tunnel data are reduced using the usual yaw force and moment coefficient nomenclature and sign convention rather than that typically associated with Magnus data. This means that, looking upstream, yaw forces are positive to the right and yaw moments tend to rotate the nose to the right. The moments are referred to the model base.

The only assumption made in reducing the data is that the yaw force and moment are zero when the angle of attack and spin are simultaneously zero. A correction resulting from this assumption is applied uniformly to all data for a given configuration and test condition. This, crudely at least, removes from the yaw data various tares such as model and flow malalignment in the yaw plane.

In reducing the data, the raw data plots were generally read at about every 4,000 rpm except when more frequent intervals were required to adequately define the trends. However, as a result of this discrete-point data reduction, the final reduced data do not present the same smooth trends and appearance that were inherent in the analog raw data plots. The reading errors and other accuracy affecting factors give an approximate overall accuracy for the wind tunnel data as follows:

$Re_L \times 10^{-6}$	$\frac{pd}{V}$	$C_Y$	$C_n$
2	$\pm 0.005$	$\pm 0.0010$	$\pm 0.0020$
4	$\pm .005$	$\pm .0005$	$\pm .0010$
6	$\pm .005$	$\pm .0003$	$\pm .0005$

Obviously these inaccuracies can be an appreciable percentage of some of the relatively low values of yaw data associated with these tests and

will make it impossible to analyze minor variations in the data. However, in spite of the level of the inaccuracies and the appearance caused by the discrete-point data-reduction procedure, the important trends shown in the data are quite clear.

## 2.5 Results and Discussion

2.5.1 General. The wind tunnel results are for models with exaggerated serrations when compared with actual bullet engraving. As stated previously the exaggerated serrations were used in these initial tests to help assure that measurable effects or trends would be obtained. Although admittedly accentuated, these trends should have some general implications with respect to the behavior of actual bullets. However, these implications are considered in other sections and only the basic wind tunnel results are presented and discussed in this section.

The wind tunnel results are presented in the form of yaw force and moment coefficients,  $C_Y$  and  $C_n$ , as functions of the nondimensional spin rate,  $\frac{pd}{V}$ . It is felt that the presentation of the data in this basic coefficient form will make the trends and effects due to the serrations more readily understood. It should be recalled (and kept in mind) that even though the yaw forces and moments act in the horizontal plane they are caused by model and aerodynamic asymmetries which occur as the model is moved to angles of attack in the perpendicular plane.

2.5.2 Comparison of Serrated and Nonserrated Model Results. The cone-cylinder data were obtained on both serrated and nonserrated models at a Mach number of 1.5 and a Reynolds number (based on the model length) of  $5.1 \times 10^6$ . A comparison of typical results for these two models is shown in Figure 3 where  $C_Y$  is plotted as a function of  $\frac{pd}{V}$  with  $\alpha$  as the parameter. The nonserrated results shown are for the model with a rather prominent sand-band boundary-layer trip to fix the transition point on the model and assure turbulent flow over the greater portion of the model. It was felt that this would more closely simulate the turbulent boundary-layer condition of the serrated model. (Nonserrated tests without the boundary-layer trip gave similar results except that the

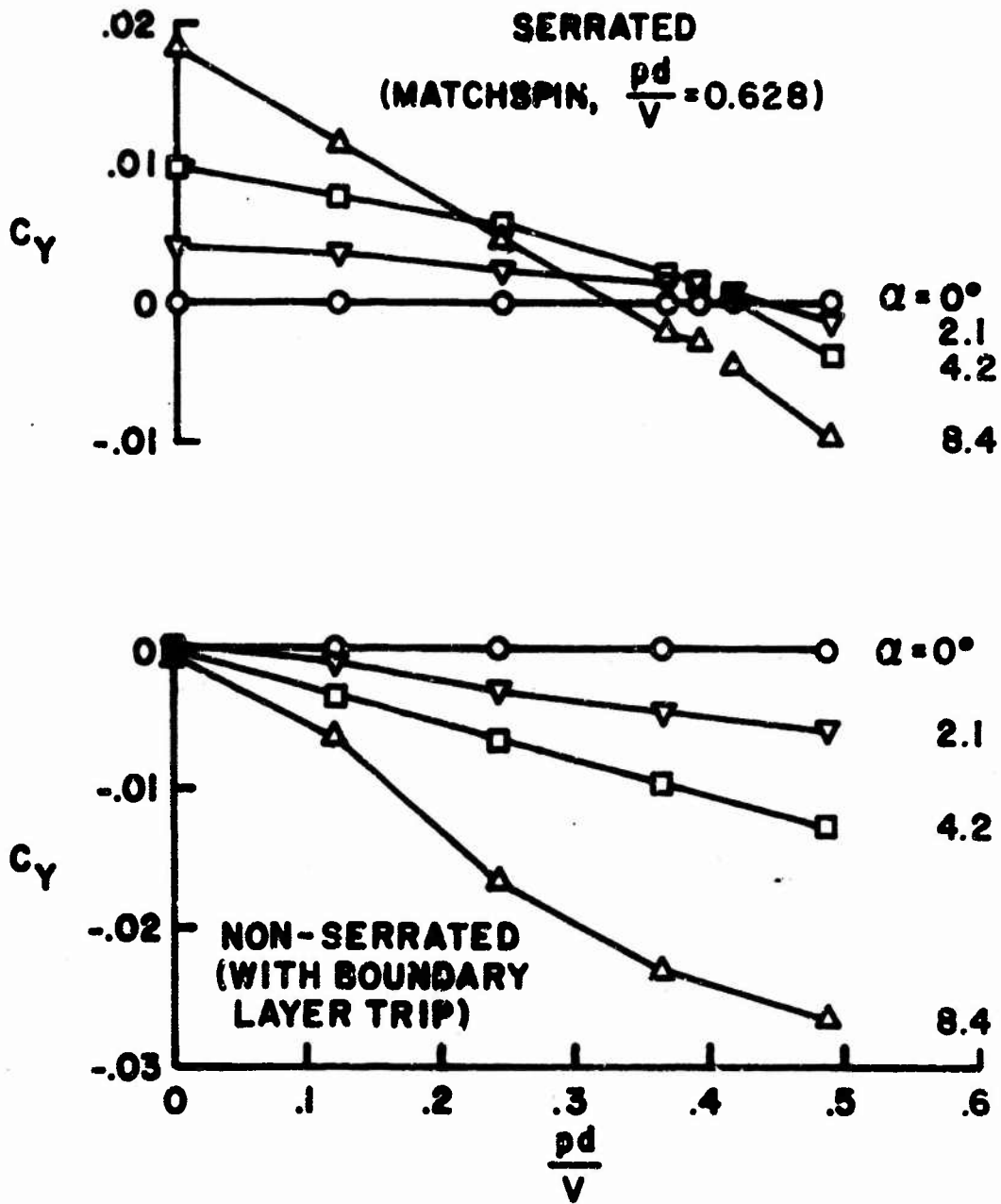


Figure 3. Comparison of Typical Serrated and Nonserrated Results for the Cone-Cylinder Models:  $M = 1.5$ ,  $Re_L = 5.1 \times 10^6$

magnitude was somewhat reduced. Such a reduction has been noted previously in reference 6.)

Basic differences, as well as similarities, in the data for the serrated and nonserrated models are immediately obvious in Figure 3. The curves for the nonserrated model indicate typical Magnus characteristics: i.e., zero side force at all angles of attack for zero spin; and then approximately linearly increasing side force, for angles of attack other than zero, as the spin rate increases. The serrated results, at zero spin, show zero side force only for zero angle of attack. At angles of attack other than zero, the serrated results indicate a side force even at zero spin. The main cause of this side force at zero spin is apparently due to the geometric and aerodynamic asymmetries associated with the serrations when the models are at angle of attack since the sign is opposite to that which would occur due to blanking out of the serrations on the lee side of the body.

As the spin rate increases, the behavior of the serrated results is very similar to those of the nonserrated model and have about the same negative slopes for corresponding angles of attack. This would suggest that the initial offset of the serrated results, due to asymmetries, is eventually overcome or relieved by an opposing "Magnus-type" force as the model spin increases. At the higher spin rates, the side force actually goes to zero at  $\frac{pd}{V} \approx 0.4$  and then becomes negative. The significance of the fact that the side force goes to zero at this value of  $\frac{pd}{V}$  is not apparent at this time. It is probably just coincidence that this value is also about the same as that for the experimental free-spin rate shown by the breaks in the curves. It might be noted that the experimental free-spin rate was approximately the same whether approached from below or above if sufficient time were allowed. However, to speed up the testing, equalization time was not allowed and consequently the values do not overlap. (Tests showed that the experimental free-spin rate increased slightly with angle of attack but more noticeably with dynamic pressure.)

Unfortunately, the twist of the serrations on this initial model was too great, 10 calibers per turn ( $2 \tan \delta = 0.628$ ), to allow testing up to the matchspin condition,  $\frac{pd}{V} = 0.628$ . Therefore, all the results shown for this model are in the so-called underspin condition. The fact that the experimental free-spin rate is considerably less than the matchspin condition is mainly attributable to the mechanical damping of the bearings and the aerodynamic roll damping.

Only the yaw force coefficient data have been presented and compared here for sake of brevity but similar trends were apparent for the yaw moment also. The yaw force center of pressure was approximately 0.5 caliber ahead of the model base for the serrated model and about 1.25 calibers for the nonserrated model.

The normal force coefficients were approximately 10 percent greater for the serrated model than for the nonserrated model but were not measurably affected by spin. The normal force center of pressure was 2.75 calibers forward of the base for the nonserrated model and about 0.1 caliber more rearward for the serrated.

Although the results of the tests on the cone-cylinder research models were of considerable interest, they were preliminary in nature and suffered from two basic limitations. One of these involved the somewhat unrealistic shape when compared to a typical bullet. The other, and more serious limitation, involved the inability to spin the model up to, and above, the matchspin condition.

The A-N spinner model with serrations only on the cylindrical section was selected as a more realistic shape for the second and more extensive set of tests. The twist was reduced to 40.7 calibers per turn,  $2 \tan \delta_g = 0.154$ , in order to provide an overspin capability. Since measurable results had been easily obtained on the deeply-grooved cone-cylinder model, the depth of the serrations on the A-N spinner was reduced by nearly 50 percent. Except where specifically noted, all serrated A-N spinner results are for tests without a boundary-layer trip. This was felt to be appropriate since the Reynolds number for the wind

tunnel tests covered the range for typical bullets. The data are for Mach number 2.0 only.

A comparison of some A-N spinner serrated and nonserrated results is shown in Figure 4. These results are for angles of attack and Reynolds number comparable to those for the cone-cylinder tests but at Mach number 2.0. Only the serrated results were obtained during the present tests. The nonserrated results were taken from reference 7. These A-N spinner results show characteristics very similar to those discussed previously for the cone-cylinder model in spite of the many apparent differences in models and test conditions: side forces at zero spin; a decrease of these side forces to zero as the spin rate increases; and experimental free-spin rates ( $pd/V \approx 0.105$ ) of approximately two-thirds the matchspin rate,  $pd/V = 0.154$ . The major difference in the comparisons is that the negative slope of the A-N spinner data is less for the serrated model than for the nonserrated whereas the slopes were about the same in the cone-cylinder case.

The serrated A-N spinner data extends to more than twice the matchspin condition of 0.154 but, at least at the higher angles of attack, there are no other identifiable trends not already pointed out. At angles of attack of 2.1 and 4.3 degrees a slight "s" shaped nonlinearity appears in the yaw force data and, although not shown here, even more prominently in the yaw moment data. These deviations from linearity will be discussed in more detail in a later section. Again, the normal force and pitching moment were not noticeably affected by spin.

2.5.3 Correlation for Different Amounts of Serration Twist. The serrated cone-cylinder and A-N spinner 4.3 degree angle of attack data from Figures 3 and 4 are replotted in Figure 5 in order to make the similarities in these data somewhat easier to visualize. In addition, data for corresponding negative angles of attack are included for completeness. In the upper part of Figure 5, the yaw data are again plotted as functions of the nondimensional spin rate and the matchspin condition is indicated for each of the two different model twist conditions. If the

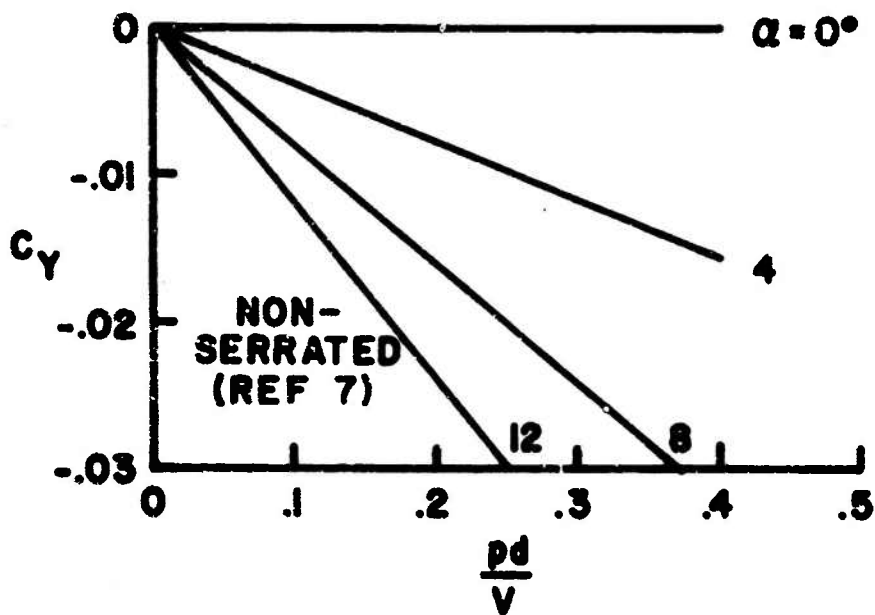
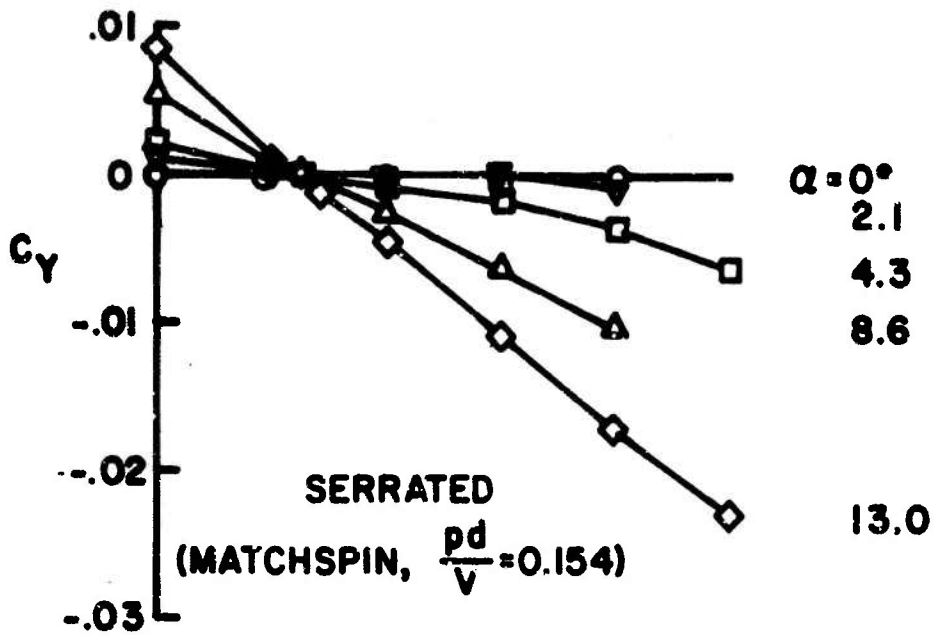


Figure 4. Comparison of Serrated and Nonserrated Results for the A-N Spinner:  $M = 2.0$ ,  $Re_p = 4.0 \times 10^6$

CONFIG	LENGTH CAL	$\theta$	M	$RO_{\rho} \times 10^{-6}$
○ CONE-CYL	5.115	17° 26'	1.5	5.1
□ A-N SPINNER	5.0	4° 25'	2.0	4.0

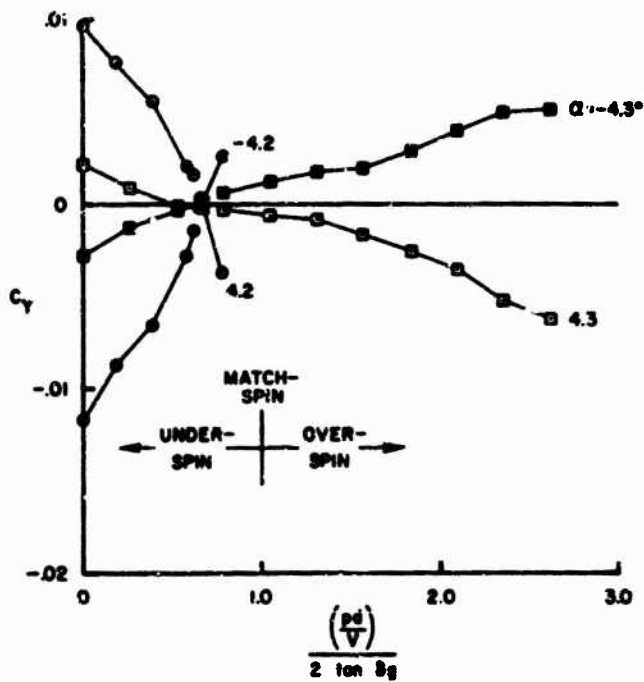
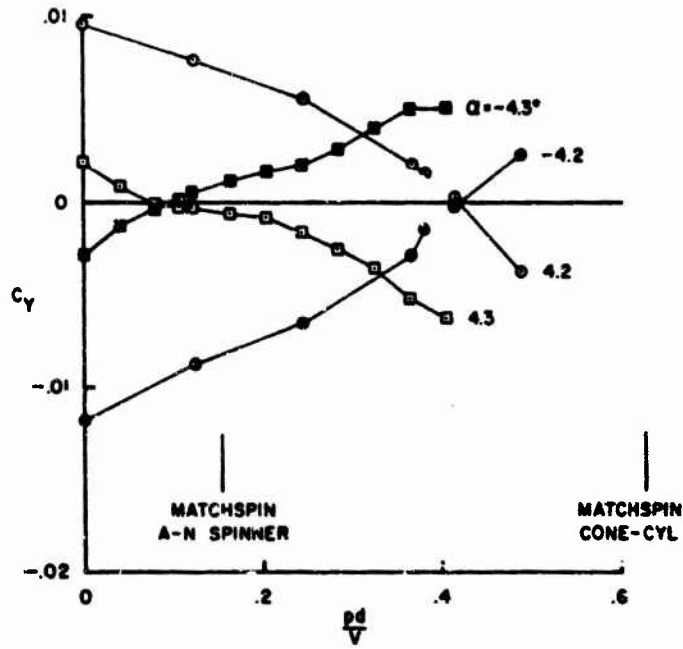


Figure 5. Comparison of Serrated Cone-Cylinder and A-N Spinner Data

data are compared in reference to their matchspin conditions, the similar characteristics discussed previously are even more apparent. This suggests the use of the factor " $2 \tan \delta_g$ " to correlate the data for models with different twist. In the bottom part of Figure 5, the nondimensional spin rate has been divided by this factor. This tends to collapse the data to a common reference on the spin axis and the matchspin condition, 1.0, applies to both models. In addition, underspin ( $< 1.0$ ) and overspin ( $> 1.0$ ) are easily identified and common for any twist. The higher magnitude of the cone-cylinder yaw force coefficients is probably mostly due to the greater serration twist and depth and, perhaps also, to the lower Mach number.

#### 2.5.4 Additional Serrated A-N Spinner Yaw Data Characteristics.

Besides the limited data presented in the previous sections for the cone-cylinder and A-N spinner models, rather extensive additional data were obtained for the serrated A-N spinner model. Although the data have not been completely analyzed and their implications are not fully apparent at this time, some of the more prominent and interesting aspects are presented and discussed in this section.

Some yaw force coefficient trends for several angle of attack ranges are shown in Figure 6 for a Reynolds number of  $4 \times 10^6$ . The top graph shows the generally linear data associated with the higher angles of attack ( $4.3$  to  $13$  and  $-4.3$  to  $-8.6$  degrees). This includes most of the data presented for the serrated A-N spinner model in the previous sections and the characteristics of this group of data have already been discussed. The slight "s" shape of the  $\pm 4.3$  degree data, which was referred to previously, is even more obvious in this plot with the expanded yaw force coefficient scale. It appears that there is a tendency for the slope and magnitude of the data to be reduced at spin rates in the vicinity of the matchspin condition. This tendency is even more obvious in the middle group of curves for angles of attack from  $\pm 4.3$  down to  $\pm 1.1$  degrees. And finally, for angles of attack of  $\pm 1.1$  degrees or less (bottom graph), the yaw force is essentially zero for

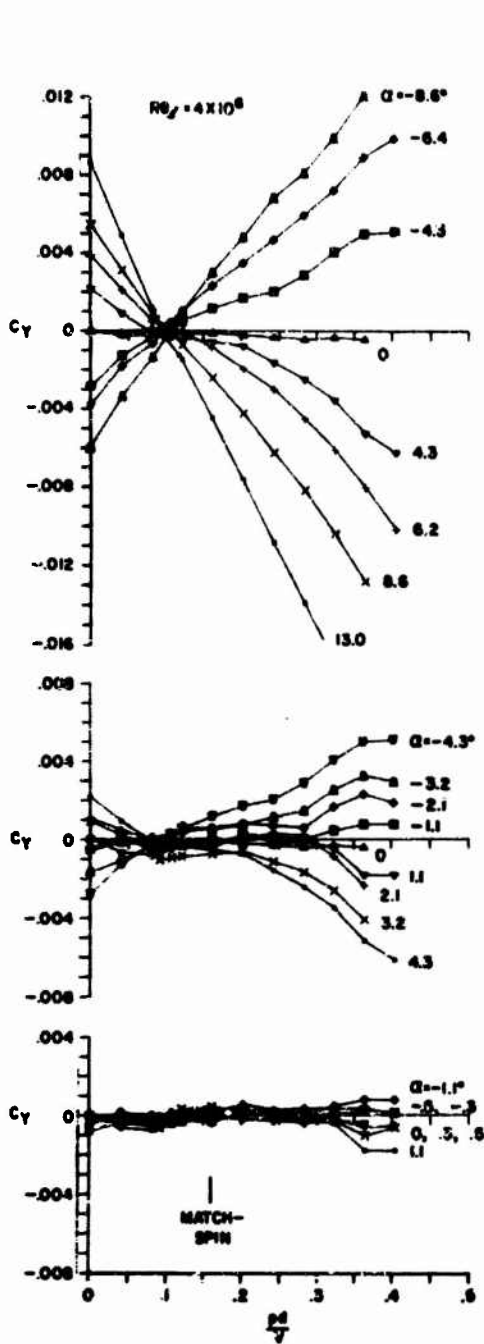


Figure 6. Serrated A-N Spinner Yaw Force Coefficient Data Trends for Several Angle of Attack Ranges at a Reynolds Number of  $4 \times 10^6$

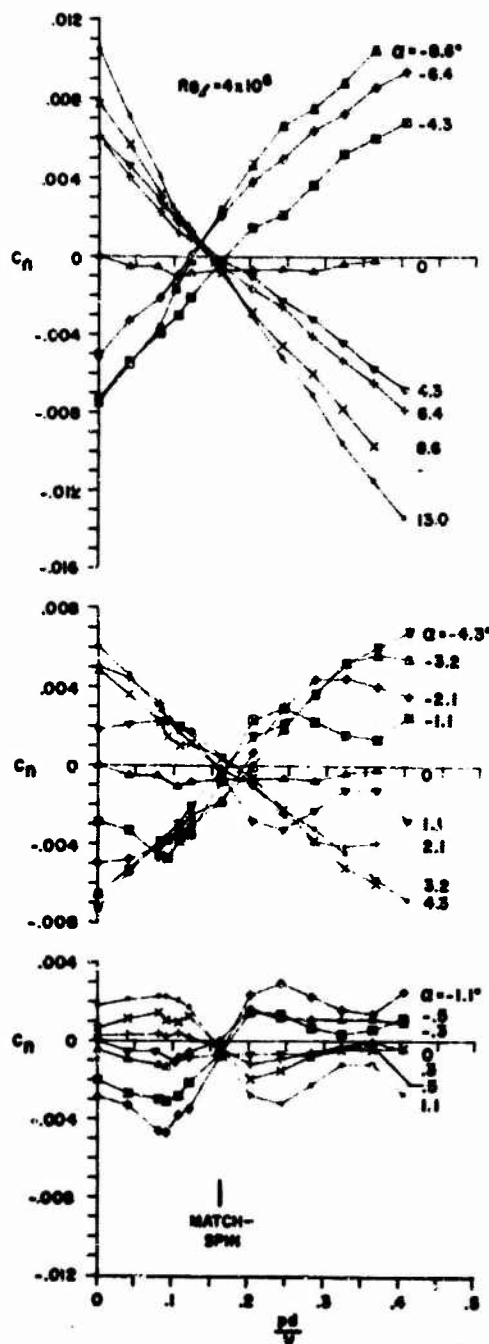


Figure 7. Serrated A-N Spinner Yaw Moment Coefficient Data Trends for Several Angle of Attack Ranges at a Reynolds Number of  $4 \times 10^6$  (Moments Referred to Model Base)

spin rates up to  $\frac{pd}{V} = 0.32$ . Therefore, for a Reynolds number of  $4 \times 10^6$ , the yaw force coefficient data are mostly linear with spin rate (except for the deviations just discussed for lower angles of attack) and the slope reduces, fairly consistently, to zero as the angle of attack is reduced to about 1.0 degree.

Now consider the corresponding yaw moment coefficient data which is plotted in Figure 7 (moments referred to model base). For the higher angles of attack (top part of figure), the trends are similar to those for the yaw force coefficient except that zero values occur (on the average) at spin rates somewhat closer to the matchspin condition. As the angle of attack is reduced from 4.3 degrees (middle graph), the linear character of the curves is gradually lost and a new and highly nonlinear form emerges at 1.1 degrees. This new form is then maintained with gradually lessening magnitudes as the angle of attack is further reduced from 1.1 to zero degrees (bottom graph).

In addition to their nonlinearity, these latter moment curves have several interesting features. First, they occur mainly for the low angles of attack where, it will be recalled, the corresponding yaw force was practically zero for values of  $pd/V$  up to 0.32. This means that a relatively pure moment is acting on the model for this spin range. In this connection, a pure yaw moment at angle of attack has also been identified for projectiles with canted fins<sup>8</sup>. Second, the moments are zero only at the matchspin condition where a sign change occurs. A marked degree of symmetry about this point is also exhibited, thus, further verifying its significance. Third, although the maximum values of the moments are not large, the slopes near the matchspin point are comparable to those for much higher angles of attack (8 to 13 degrees). And finally, a short, but relatively linear, section persists near the matchspin condition.

Tests at higher Reynolds number ( $6 \times 10^6$ ) and tests with a sand-band boundary-layer trip did not indicate any change in the general character of the results. These results should be pertinent for small caliber

projectiles with lengths of 4 inches or more since sea level Reynolds numbers are approximately equal to  $1 \times 10^6$  per inch of projectile length.

For smaller projectiles at sea level, the results in Figures 8 and 9 should be of more significance. These data are for a Reynolds number of  $2 \times 10^6$  and are presented for three different ranges of angle of attack in a manner analogous to that just discussed for the higher Reynolds number results. For clarity, however, only positive angles of attack are plotted.

In Figure 8, the yaw force coefficient trends at the higher angles of attack (top graph) are similar to those mentioned for the higher Reynolds number except that the tendency toward nonlinearity, as the angle of attack is reduced, is somewhat more prevalent and already quite pronounced by 4.1 degrees. At angles of attack between 4.1 and 1.0 degree (middle graph), transition to yet another class of phenomenon occurs. The yaw force coefficient curves pass from the somewhat erratic but generally neutral levels at 2.1 degrees angle of attack to an accentuated "sine-wave" shape at 1.0 degree. This characteristic shape then remains dominant at the still lower angles of attack as shown in the lower portion of the figure. Again the curves appear to be approximately symmetrical about a point near or slightly above matchspin. Also of particular significance, considering the fact that the angles of attack are 1 degree or less, are the relatively large values of yaw force coefficient for small amounts of spin mismatch as well as the extremely steep slopes and sudden slope reversals.

The corresponding yaw moment coefficient behavior is shown in Figure 9. In addition to showing some of the characteristics of the related yaw force data, an even more complex behavior occurs near the matchspin point at angles of attack of 0.3 to 0.5 degree (bottom graph). Also the "sine-wave" type of trend in the moment data (at  $\alpha = 1.0$  degree, for example) is modified in such a way that it cannot be explained solely by the yaw force (of Figure 8) acting at some distance from the moment reference. It is probable that this modification is caused by a

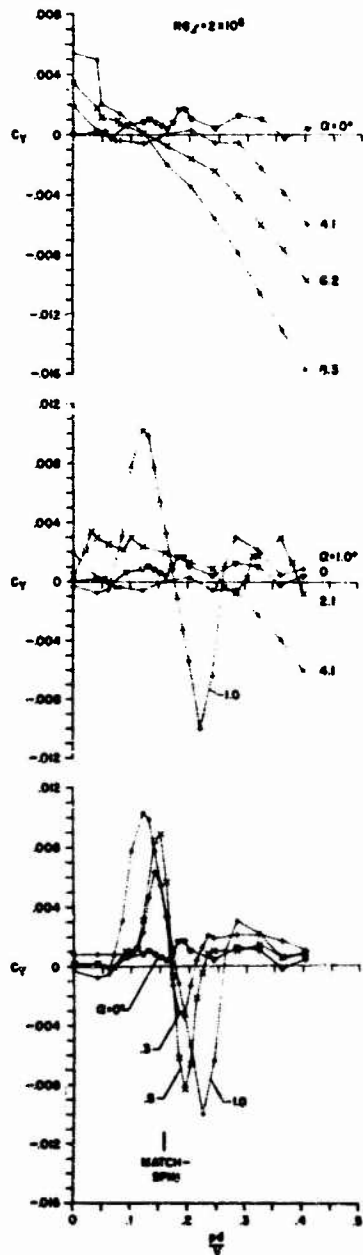


Figure 8. Serrated A-N Spinner Yaw Force Coefficient Data Trends for Several Angle of Attack Ranges at a Reynolds Number of  $2 \times 10^6$

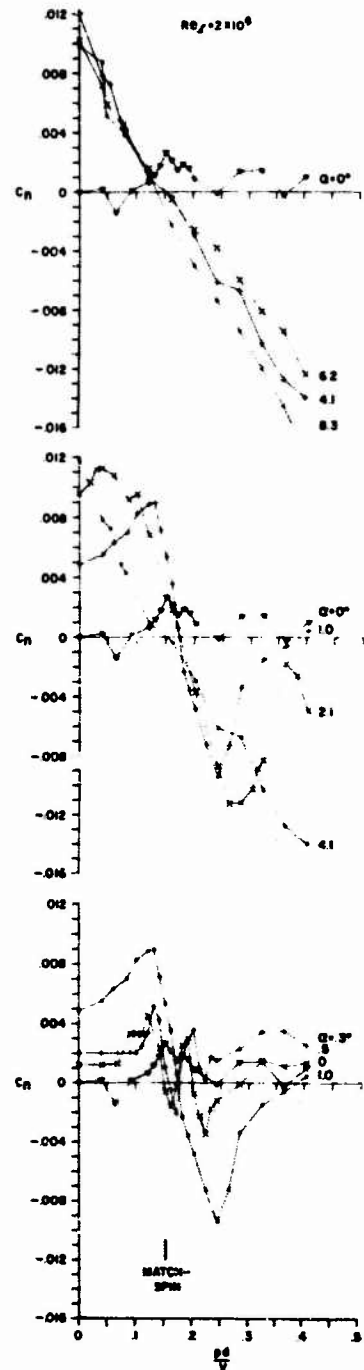


Figure 9. Serrated A-N Spinner Yaw Moment Coefficient Data Trends for Several Angle of Attack Ranges at a Reynolds Number of  $2 \times 10^6$  (Moments Referred to Model Base)

"pure-moment" effect (similar to that discussed for the higher Reynolds number data) being added to the moment due to the yaw force. This "pure-moment" addition would tend to broaden the peaks as shown by the data and explain the existence of the moment at spin rates where the yaw force is zero.

Although only the data trends for positive angles of attack are discussed in Figures 8 and 9, similar trends but opposite in sign occur for negative angles of attack. This is shown quite graphically in Figure 10 where the yaw force and pitching moment coefficients for  $\pm 1.0$  degree angles of attack are plotted on the same axis.

Some of the more dramatic trends discussed in this section are for the lower Reynolds number data ( $Re_L = 2 \times 10^6$ ). As the Reynolds number is increased, these trends are greatly attenuated and in some cases eliminated entirely as shown in Figure 11 where the yaw data for  $\alpha \approx 1.1$  degree are summarized for Reynolds numbers of 2, 4 and  $6 \times 10^6$ . Artificial tripping of the boundary layer has a similar effect as shown by the results in Figure 12. In this figure, the yaw data for  $\alpha \approx 1.0$  degree and a Reynolds number of  $2 \times 10^6$  are shown for tests both with and without the boundary-layer trip. The attenuating effect of the trip is comparable to that of increased Reynolds number. This similarity of effects would suggest that the boundary-layer characteristics with the trip and at higher Reynolds numbers might be somewhat similar. Unfortunately, this suggestion could not be verified with the available shadowgraphs of the boundary-layer flow conditions. Shadowgraphs are available only for a Reynolds number of  $4 \times 10^6$  and show that without a trip the boundary layer on the top and bottom of the model is apparently laminar up to the serrations. After being "swallowed" by the serrations it then emerges in a turbulent condition. With the trip, the boundary layer is turbulent downstream of the trip position. The data of the last two figures reemphasizes the significance of the Reynolds number or boundary-layer condition and, based only on this consideration, it would be anticipated that bullets or projectiles of about two inches or less in length ( $Re_L < 2.0 \times 10^6$ ) would probably be most affected by the yaw data characteristics shown.

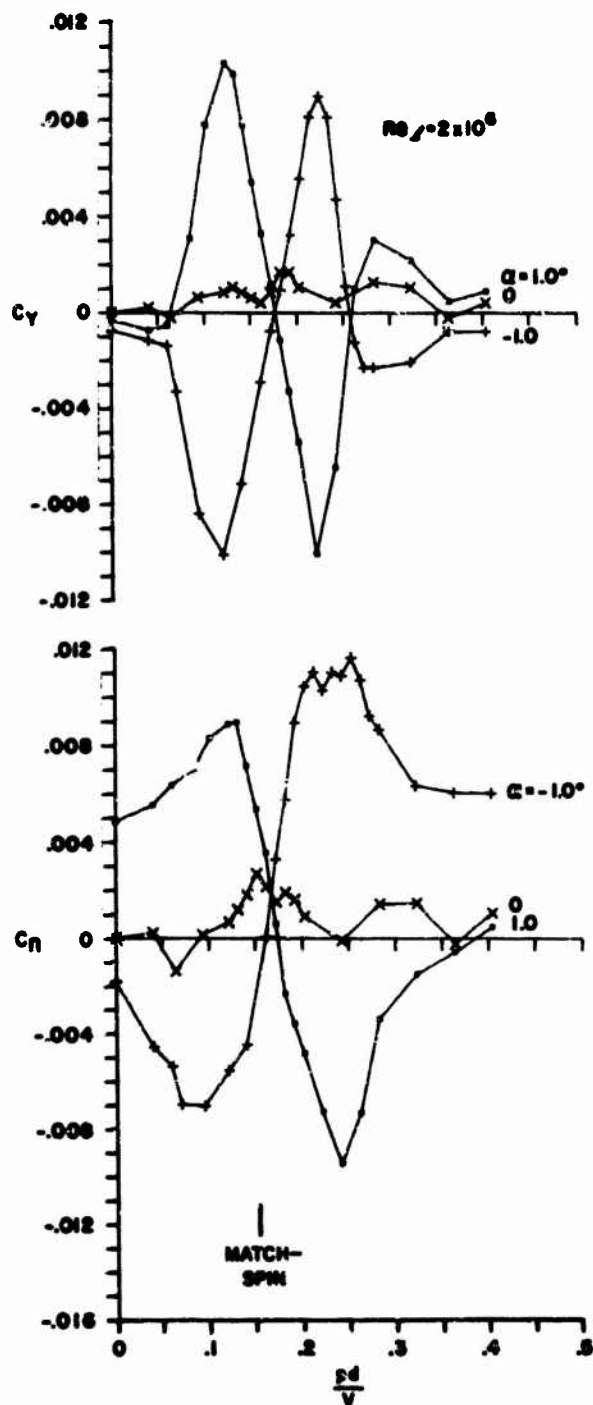


Figure 10. Serrated A-N Spinner Yaw Force and Moment Data for Positive and Negative Angles of Attack at a Reynolds Number of  $2 \times 10^6$  (Moments Referred to Model Base)

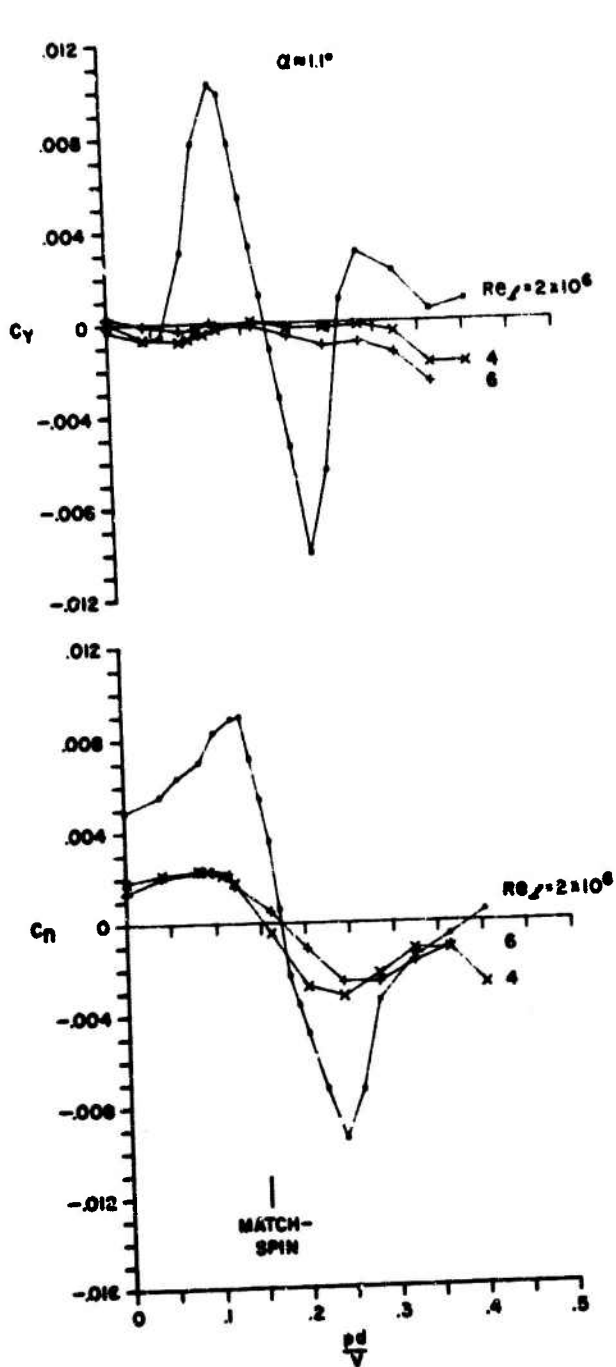


Figure 11. Effect of Reynolds Number on the Yaw Force and Moment Characteristics of the Serrated A-N Spinner:  $\alpha \approx 1.1$  Degree (Moments Referred to Model Base)

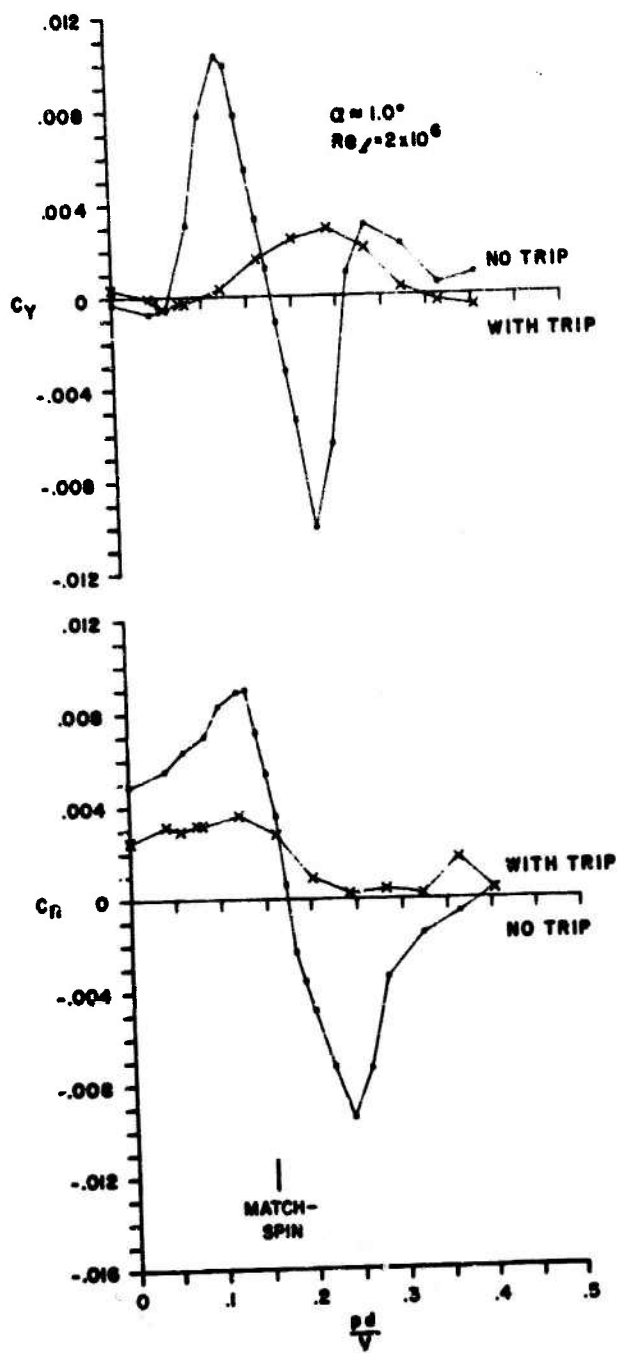


Figure 12. Effect of Boundary-Layer Trip on the Yaw Force and Moment Characteristics of the Serrated A-N Spinner at a Reynolds Number of  $2 \times 10^6$ :  $\alpha \approx 1.0$  Degree (Moments Referred to Model Base)

All of the wind tunnel test data presented and discussed are for models with rather exaggerated serrations compared to the engraving on a typical bullet. Wind tunnel tests are planned in the near future on models with more practical serration depths and spacing and an attempt will be made to provide overlapping of wind tunnel and range results. In the meantime, it is felt that the present wind tunnel results, although perhaps accentuated in magnitude, may indicate some of the complexities of the aerodynamics involved for configurations, such as bullets, with more practical departures from mirror symmetry.

### 3. FREE FLIGHT RANGE INVESTIGATION

#### 3.1 Test Facility and Routine Techniques

Flight simulation range tests were conducted in the Free Flight Aerodynamics Range at the Ballistic Research Laboratories<sup>9</sup>. Range techniques produce a time and photographic record of the bullets' flight (Figure 13). The attitude of the axis of symmetry and the coordinates of the center of gravity are used to determine the coefficients of the equation of motion of the yawing bullet. Time and distance data are used in the drag determination. So called spin-pins in the base of the bullet are used to determine the orientation about the axis of symmetry. This is used with the distance and drag data to determine spin deceleration. Ballistic force and moment coefficients for the flight are obtained from the equations of motion<sup>1</sup>.

#### 3.2 Special Techniques for Spin Mismatch Measurements

The range test facility is only 300 feet long. Since it was expected that the effects of a lack of mirror symmetry would be evident only over extended trajectories, it was felt that the usual techniques of simulating down range test conditions would be unsatisfactory in producing meaningful data. Thus, a better technique of flight simulation was needed. Since axial deceleration is generally greater than spin deceleration, the rate of spin increases with range. A true simulation would require increasing the spin of the bullet after it left the rifle.

This can be accomplished by pre-engraving the bullet and saboting it for a larger caliber, high twist rifle. There are the usual problems in the control of the yaw in these sabot methods, and in particular it is difficult to get low yaw rounds in flight.

It was suspected, and later evidence justified this supposition, that the effects of small deviations in mirror symmetry would reflect about the matchspin condition. Thus, an underspun bullet would show similar effects as an overspun bullet but with some sign reversals.

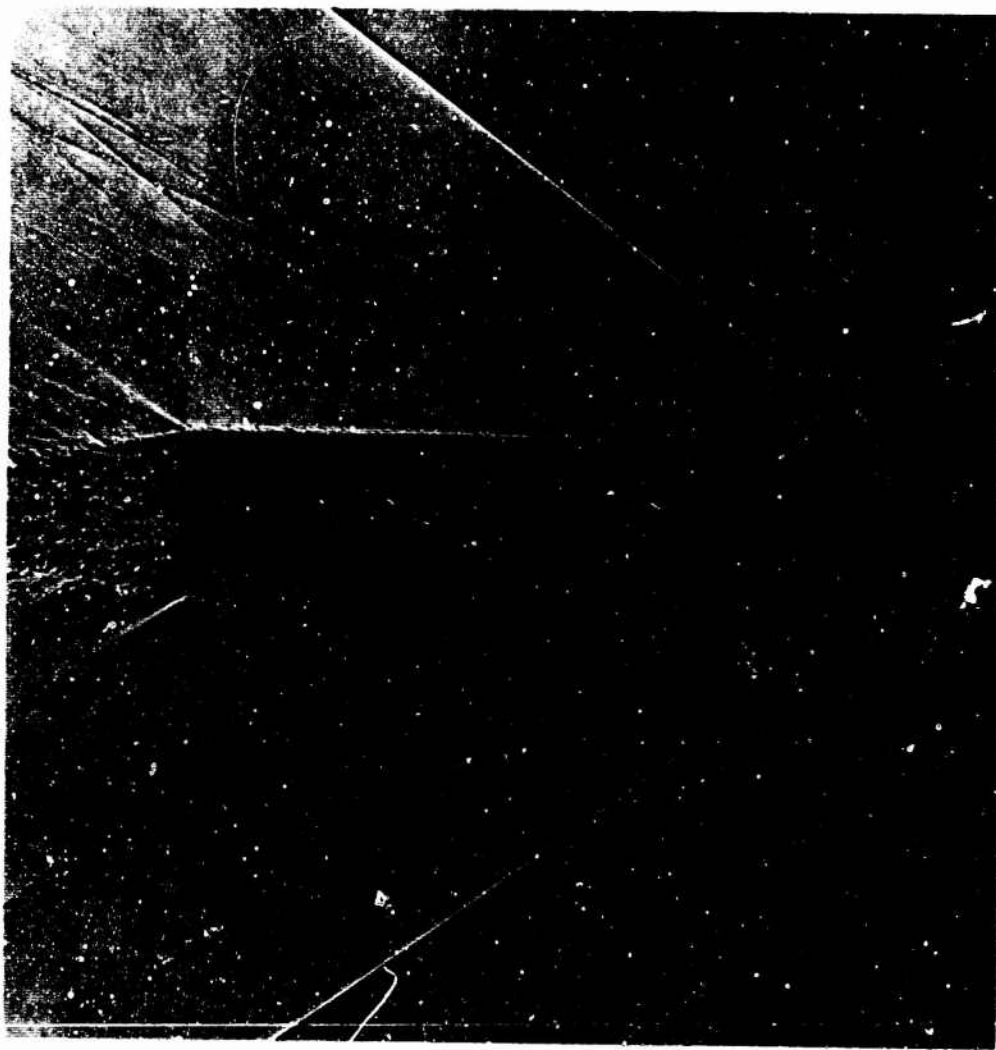


Figure 13. Spark Photograph of Pre-engraved A-N Spinner Rocket Model, Mach 1.85, Underspin Flight

A relatively simple method was available for firing the underspun bullet. Either standard lead core bullets or pre-engraved brass models can be fired from a high twist rifle. A strong electromagnet is placed close to the gun muzzle so that the two foot long magnetic field is normal to the trajectory. When the spinning bullet passes through the field, eddy currents are generated that react with the magnetic field to produce a spin decelerating torque. The field strength can be made as high as 20,000 gauss, which can reduce the spin of a caliber .30 bullet fired from a high twist gun, (.320 rad/cal) to the point where the bullet is gyroscopically unstable. This technique is so much more satisfactory in the control of the initial conditions of the bullet's flight, it was selected for the first attempt at investigating the phenomenon. Subsequent programs included the overspun condition, using sabotaged models.

### 3.3 General Test Plan

A more exact simulation of the projectile's total flight in a range test requires control of both velocity and spin, naturally with the bullet fired from the same gun type. The effects of small deviations in mirror symmetry are small and are not easily observed if at all in a single round range flight. A basic principle in the test plan is to compare at some reduced velocity the motion of rounds having a complete range of spin conditions, (1) at two values of underspin, (2) at the spin match condition, and (3) at two values of an overspin condition. The requirements of range techniques, stable flights at several levels of maximum yaw, limit the range of gyroscopic stability factors that are acceptable for a test flight. More than one engraving helix angle is required to meet all situations, to have the required spin rate to engraving angle ratio and a suitable gyroscopic stability.

Since the discrepancies between the predicted and the actual flight of the projectile had been observed at long ranges, low velocities appeared to be the more pertinent test region. Mach 1.4 was selected as an initial test point, thus avoiding the transonic region. Later tests branched out to the higher Mach numbers. Since wind tunnel data has

been taken at Mach 2, this is also a particularly useful test point. The initial detection phase program used standard ammunition. The second test plan used pre-engraved homogeneous models.

### 3.4 The Models

Since the investigation was an outgrowth of the discrepancies between the predicted and actual flight dynamics of bullets at long ranges, the first test plan involved real bullets; a square base, caliber .30 Ball M2 and the boattail, 7.62mm M80. Both of these were tested in the underspun flight condition. To avoid the scatter in the data due to the unpredictable variations in lead bullet physical dimensions, the second test plan used machined homogeneous models.

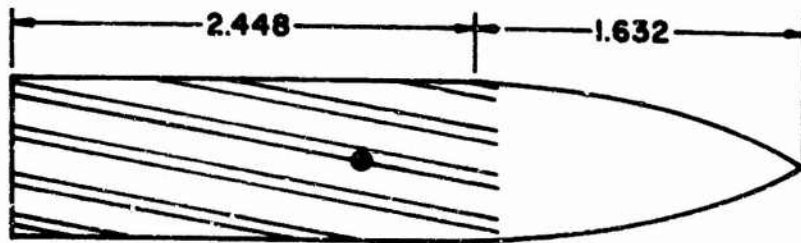
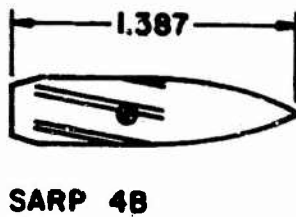
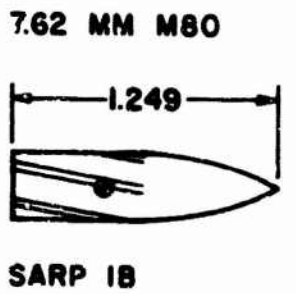
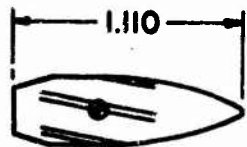
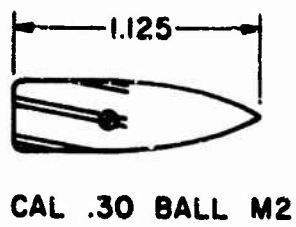
(1) The square base caliber .30 Sarp 1B, (2) the boattail caliber .30 Sarp 4B, (3) the 20mm pre-engraved 5 caliber A-N Spinner Rocket, and (4) the caliber .725 spiral grooved A-N Spinner Rocket. The models are pre-engraved for the underspun test. For the overspun test the models are subcalibered for a high twist 20mm gun. The basic bullet shapes and the rifling details of standard guns are given in Figure 14.

### 3.5 Results

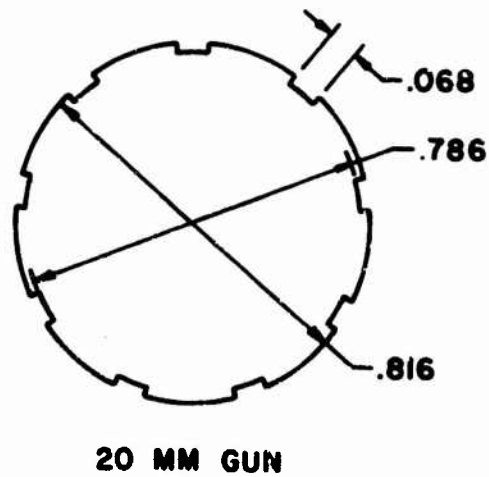
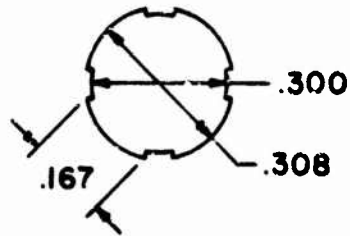
The data obtained from the rounds fired in the range were processed by methods based on the assumption of a linearized aerodynamic force and moment system<sup>1</sup>. The nonlinear trends are coupled with a partial negation of the mirror symmetry assumption. For the rolling moment coefficients these effects were investigated. For the other parameters the results are presented in the form of the linearized aerodynamic slope coefficients.

The data for the detection phase program were obtained with standard ammunition. Most of the other results were obtained from firings of Sarp 1B bronze models.

3.5.1 Detection Phase Range Program. Since the data for this program are mostly qualitative, only a brief presentation of the results will be given. Nevertheless, these tests were the basis for planning



**GUN RIFLING DETAILS**



● CENTER OF GRAVITY  
 ALL DIMENSIONS ARE IN INCHES

Figure 14. Range Test Models

others. The primary test projectiles were the square based caliber .30 Ball M2 and the boattailed 7.62mm Ball M80. These tests were at under-spin conditions using the electromagnetic spin brake. Some rounds were sabotaged and fired at the overspin condition but high yaw and large dispersion resulted and no useful data were obtained.

Despite the typical data scatter for these deformable projectiles, definite effects were observed. The coefficients determined from the reduction and normally associated with the Magnus and damping moments showed distinct differences. These were observed with the square base, caliber .30 Ball M2 and with the boattailed M80 Ball. However, the trends for the latter were different and less noticeable. For the caliber .30 M2 bullet the Magnus moment and damping moment coefficients are shown for low yaw in Figures 15 and 16.

The basic purpose of the range detection phase program was fulfilled. A measurable effect does exist due to spin mismatch for typical bullets.

3.5.2 The Static Aerodynamic Properties. Probable order of magnitude considerations implied that as long as the deviations from mirror symmetry were small, first order changes in the static aerodynamic coefficients were not expected. However, with no computable model of the aerodynamic phenomena to yield actual size estimates for the coefficients, it was considered that empirical data supporting this hypothesis for these coefficients were equally important.

Where range data are exceptionally good, trends due to higher order effects may be found. Graphs of the zero-yaw drag, the static moment and the normal force coefficients are given in Figure 17. The drag data has been corrected for yaw and for the small Mach number spread about 1.42. There appears to be no significant trends in the data. In the case of the overturning moment and the normal force coefficient, there appears to be no particular trends, except perhaps a greater spread of the data in the spin match region. If the data for the overturning moment is grouped and plotted as in Figure 18, there is shown, for the matchspin rounds, a definite trend towards a slight increase in the over-

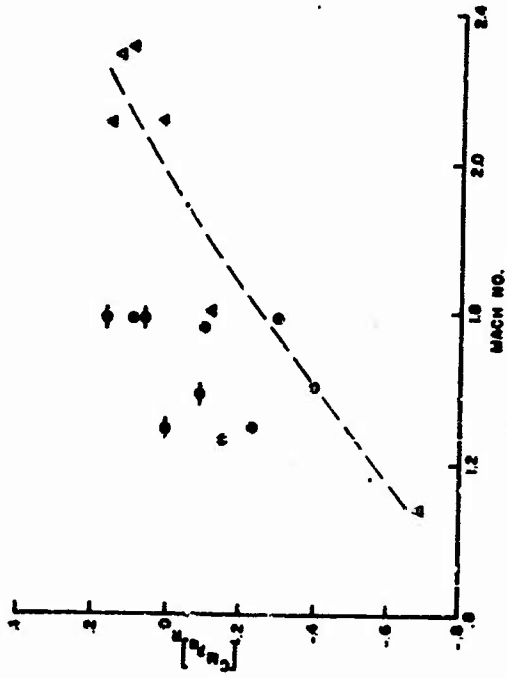


Figure 15. Magnus Moment Coefficient, Caliber .30 Ball M2, Effect of Underspin

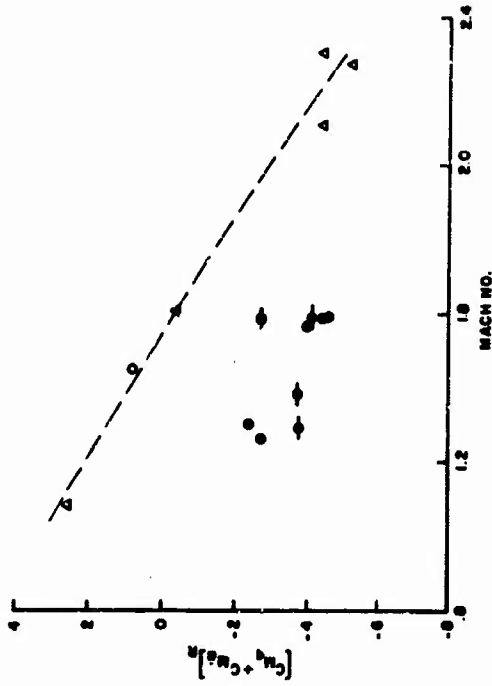


Figure 16. Damping Moment Coefficient, Caliber .30 Ball M2, Effect of Underspin

Symbol	$2 \tan \delta$ g	$\frac{pd}{V}$ , rad/cal	$\frac{pd}{V} \frac{1}{2 \tan \delta}$ g
$\Delta$	0.19	0.19	1.00
$\circ$	0.32	0.32	1.00
$\bullet$	0.32	0.22 - 0.24	.68 - .75
$\bullet$	0.32	0.13 - 0.16	.39 - .50

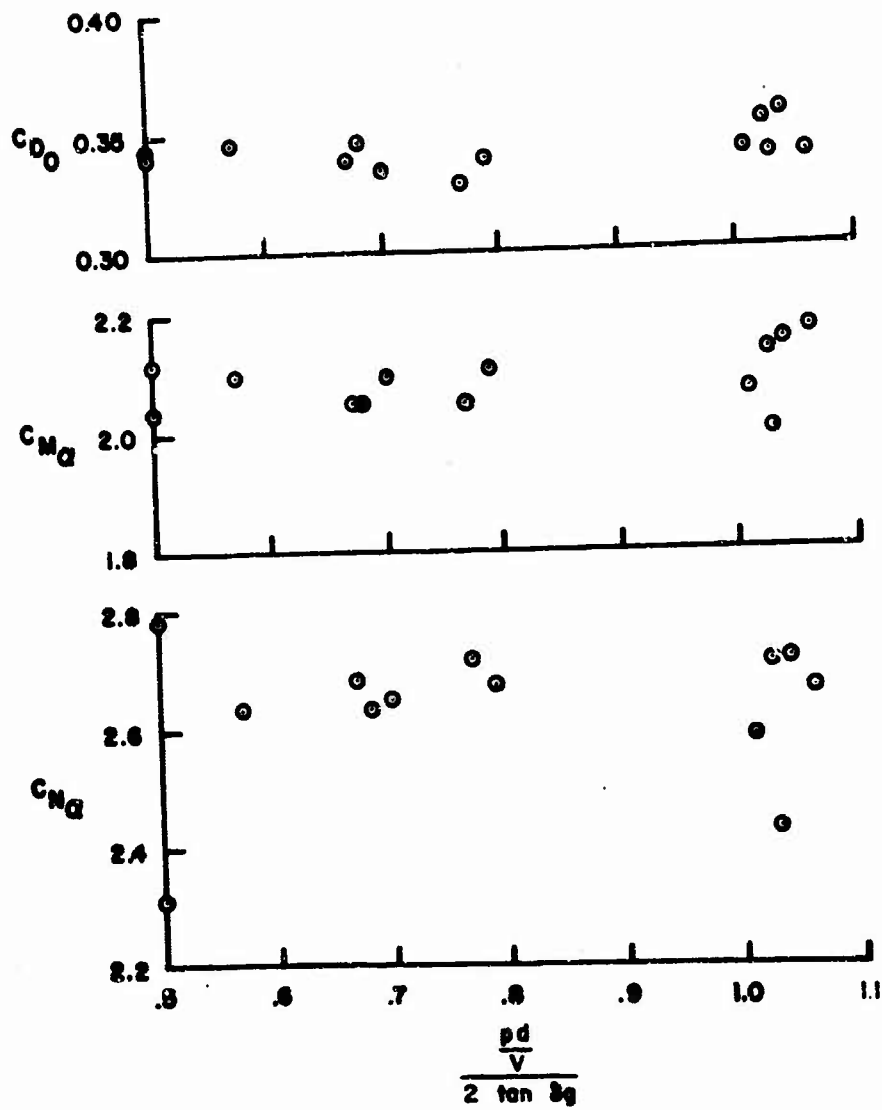


Figure 17. Static Coefficients Vs Spin Mismatch Ratio, Sarp 1B Models, Mach 1.42

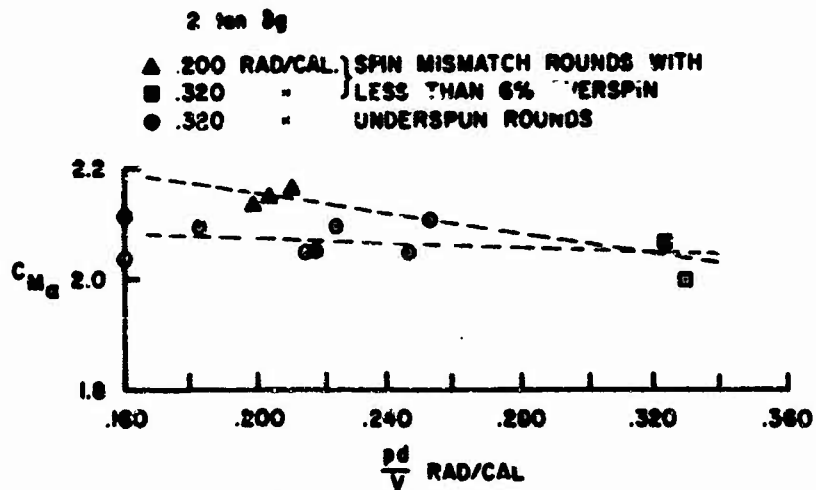


Figure 18. Static Moment Coefficient Vs Spin

turning moment with a decrease in spin. This same increase cannot be seen when the spin decrease is coupled with spin mismatch.

The data shown are for the caliber .30 S&W 1B bronze models. Preliminary results from range tests of the A-N Spinner Rocket models also give negative results and these are in agreement with the wind tunnel data.

**3.5.3 The Magnus and Damping Moments.** The initial detection program showed the need for revising the dynamical equations of motion to take into account the breakdown in the mirror symmetry assumption. This, of course, adds a large number of terms many of which we expect will have a negligible contribution because of the minor nature of the discrepancy. The data presented in Figures 19 and 20 refer to the computed values of the coefficients derived with a mirror symmetry assumption. There are strong nonlinearities with yaw coupled with the spin mismatch effect. This is indicated on the graphs by the curves which show the general yaw levels of the data points. The low yaw trends are similar to those for caliber .30 Ball M2 rounds mentioned previously in Figures 15 and 16.

**3.5.4 The Rolling Motion.** The aeroballistic range test data produces the angular orientation and the distance along the trajectory from the spark photographs of the roll pins located in the base of the model. For shell, bullets and their models, the general equation of motion is taken to be:

$$I_x \dot{p} = \frac{1}{2} \rho V^2 S d \left( \frac{pd}{V} \right) C_{L_p} . \quad (1)$$

For a wind tunnel test where the velocity can be a constant, solution is:

$$p = p_0 e^{-Ct} . \quad (2)$$

This implication that the spin damps to zero is obviously not consistent with an experiment using a model having simulated engraving, or helical

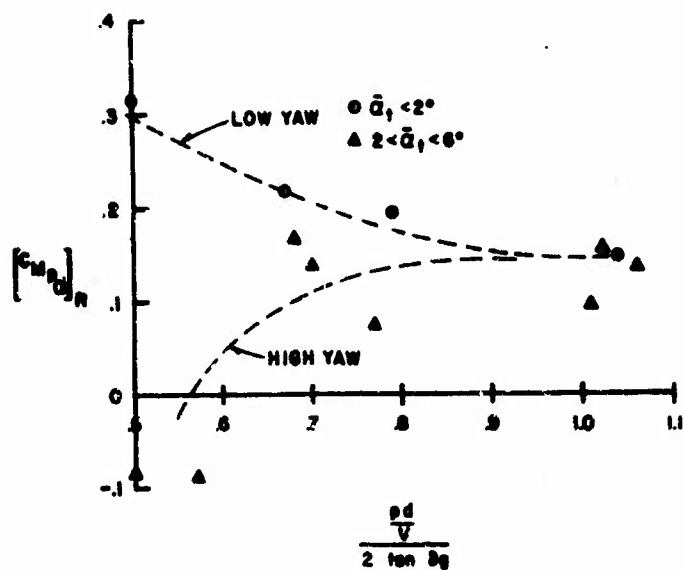


Figure 19. The Magnus Moment Coefficient, Sarp 1B Model, Mach 1.42

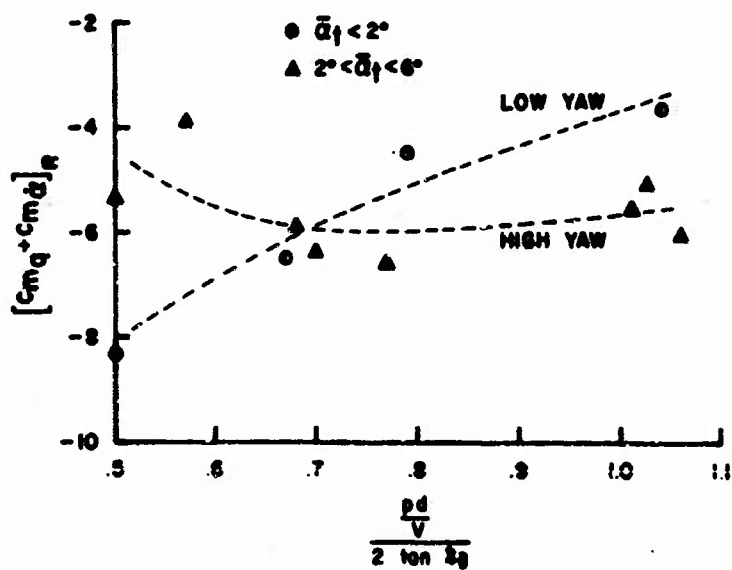


Figure 20. The Damping Moment Coefficients, Sarp 1B Model, Mach 1.42

grooves. A serrated model was permitted to coast to its steady state spin from the overspin condition, 36,000 rpm and to be driven by the helical grooves from the underspun condition 0 rpm. Spin data was recorded as a function of time (Figure 21). The spin increase and decay curves are essentially functions of at least three torques caused by (a) the aerodynamic roll damping moment due to rolling velocity, (b) the roll moment due to the helical grooves or the spin mismatch, (c) a roll damping moment due to the mechanical bearing loads and friction. While it is not possible to separate the size of the three torques in the particular test, it is evident that the torques due to the helical grooves are at least of the order of magnitude of the torque due to rolling velocity. This suggests that the formulation for the rolling motion of finned missiles is more appropriate for bullets. The additional term in the finned missile formulation is simply a consequence of the non-mirror symmetry assumption. However, the effects of the minuscule "fins" or the engraving produced by the gun has had little impact for ballistic range data obtained within 300 feet of the gun muzzle. The basic structure of these "fins" negates the assumption of mirror symmetry. But its effects on the roll moment cannot be adequately determined for small arms bullets over this short test trajectory. What little effects that do exist are absorbed in the  $C_{L_p}$  terms which, for the rifled bullet, is slightly larger than that of an equivalent smooth body. For the single test round, it cannot be shown whether the increase in the  $C_{L_p}$  coefficient is due to the roughness associated with the engraving or due to the lack of mirror symmetry. Since the single round cannot produce adequate data, the data bank was composed of many rounds with the same twist of rifling, and the same velocity but different spin rates.

It seems inappropriate to describe the bullet engraving as fins. Thus, we modify the roll equation slightly and redefine the nature of the roll moment coefficient. Instead of a roll moment coefficient due to canted fins, we use a roll moment coefficient due to spin mismatch. The equation for rolling motion of the bullet becomes:

$$I_x \dot{\phi} = \frac{1}{2} \rho V^2 S d \left\{ (\tan \delta_g - \frac{pd}{2V}) C_{l_\delta} + \frac{pd}{V} C_{l_p} \right\} \quad (3)$$

For a constant drag coefficient, changing the independent variable to distance gives a linear equation with constant coefficients.

$$\phi'' + K_p \phi' - K_\delta = 0 \quad (4)$$

where

$$\phi' = \frac{pd}{V}$$

$$K_p = -\frac{\rho S d}{2m} [k_a^{-2} (C_{l_p} - \frac{1}{2} C_{l_\delta}) + C_D]$$

$$K_\delta = +\frac{\rho S d}{2m} k_a^{-2} \tan \delta_g C_{l_\delta}$$

For a single range flight, since  $K_p s$  is small, the exponential in the solution of equation (4) can be expanded as a cubic:

$$\phi = \phi_0 + \phi'_0 s + \frac{1}{2} (K_\delta - \phi'_0 K_p) s^2 - \frac{1}{6} K_p (K_\delta - \phi'_0 K_p) s^3 \quad (5)$$

From a least square fit of the measured angles and distance data to the cubic equation, a total spin moment coefficient is obtained from the quadratic and linear terms.

$$[C_{l_p}]_R = \frac{2 \tan \delta_g - \phi'_0}{2 \phi'_0} C_{l_\delta} + C_{l_p} \quad (6)$$

Thirteen rounds were fired with the spin mismatch term  $\left( \frac{2 \tan \delta_g - \phi'_0}{2 \phi'_0} \right)$

varying from +0.5 to -0.1. A plot of the total roll damping moment coefficient data against the spin mismatch term indicated a strong yaw

effect on damping at high values of spin mismatch. The effects of yaw on the roll moment coefficient due to rolling velocity has only rarely been detected in range measurements. Since the functional dependence of drag is well represented by a quadratic in yaw, a similar representation was used for the spin mismatch coefficient to remove the yaw effect. This is shown in Figure 22.

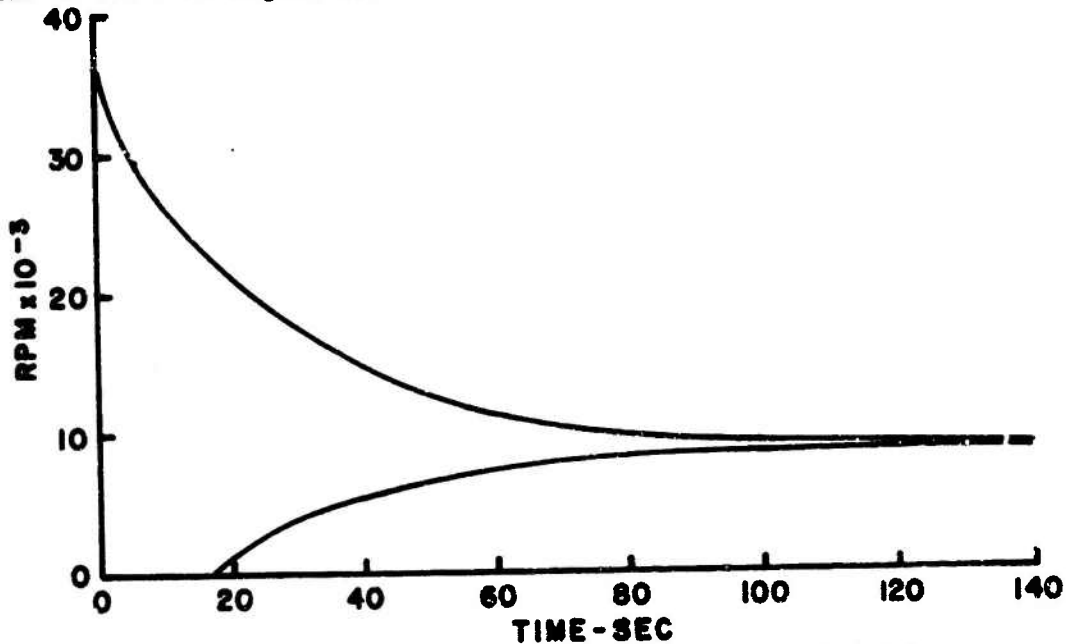


Figure 21. Roll Damping, Free Spinning Serrated Model

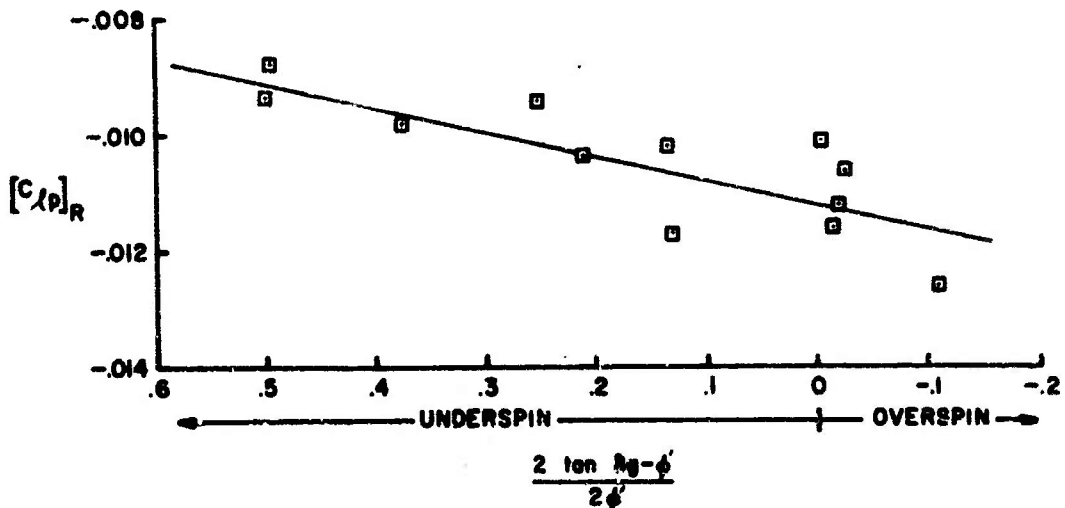


Figure 22. Rolling Moments, Caliber .30 Sarp 1B Model, Mach 1.42

At small yaw levels, the total roll damping coefficient decreased 20 percent when the underspin term was one-half. Where large yaws are encountered, a decrease of as much as 50 percent has been observed. At long ranges the mirror image of this flight condition occurs, and the spin rate can be as much as four times the engraving angle. The effect of spin mismatch and yaw at long range would be to increase the total roll damping.

3.5.5 The Damping Coefficients. In the discussion of the aerodynamic properties, the possible impact of the spin mismatch phenomena on the stability properties of the projectile is not evident. One of the observed discrepancies was in the damping behavior. The measured exponential damping coefficients of the bronze bullet models, Figure 23, show an increase in the damping of the fast mode with an increase in

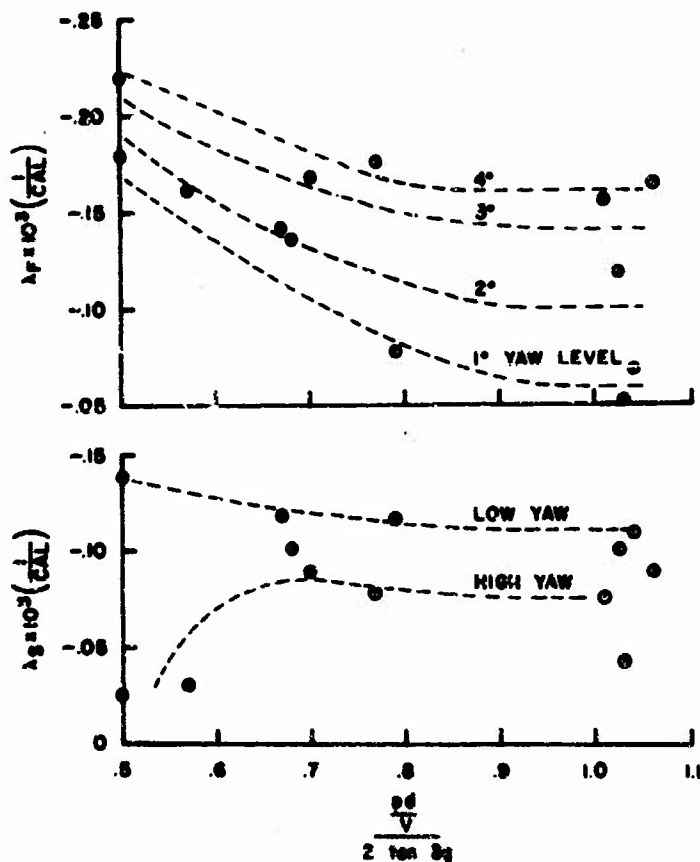


Figure 23. The Exponential Damping Coefficients, Sarp 1B Models

underspin. The yaw levels are indicated on the graph. At low yaw there is a similar trend for the slow mode damping. However, at the high yaw levels the slow mode damping does not follow this trend. It is clear that these effects might be extrapolated only with caution until the phenomena is better understood. The general picture does exist, however, that the underspin cases are more stable than the matchspin condition. This suggests that the overspin condition is less stable. The wind tunnel results suggest a more complicated picture at higher spin ratios.

#### 4. CONCLUSIONS

Wind tunnel tests on spinning models with exaggerated helical serrations have shown that the aerodynamic characteristics can be very complex and quite different than the Magnus characteristics associated with similar but nonserrated models. Yaw forces and moments occur at angles of attack even at zero spin. As the spin increases, the trends of the yaw forces and moments can be linear at higher angles of attack or very nonlinear at lower angles of attack. The trends are quite sensitive to the Reynolds number and the boundary-layer condition, and exhibit the more extreme behavior at lower Reynolds numbers. A strong tendency for symmetry of the data trends about the matchspin condition is shown to exist, thus establishing the significance of this parameter. On the basis of these results, it is speculated that similar but more subdued effects may occur on bullets with less prominent engraving.

The range phase one detection tests with standard ammunition have shown that the underspin flights produce measurable differences in the Magnus and damping moment coefficients when they are compared with matchspin flights.

For the roll moment, of a bullet model with small deviations from mirror symmetry, the equation for the rolling motion of a finned missile is modified slightly, requiring additional coefficients to describe the roll damping. For a model of a particular bullet, values of these coefficients are obtained.

Little change is observed for the drag, overturning moment and the normal force coefficients.

At low yaw, the Magnus moment coefficient increases with large value of underspin. This trend does not appear to hold for flights with large yaw. The damping moment coefficients appear to be strongly dependent on yaw as well as spin mismatch. The fast mode exponential damping increases with underspin. A yaw effect could be observed. For the slow mode this same increase occurs with low yaw. At higher yaw levels the damping decreases.

## REFERENCES

1. C. H. Murphy, "Free Flight Motion of Symmetric Missiles," Ballistic Research Laboratories Report No. 1216, July 1963. AD 442757.
2. R. E. Bolz and J. D. Nicolaides, "A Method of Determining Some Aerodynamic Coefficients from Supersonic Free-Flight Tests of a Rolling Missile," Ballistic Research Laboratories Report No. 711, December 1949. AD 801752. Also, J. Aero. Sciences 17, pp. 609-621, October 1950.
3. J. D. Nicolaides, "On the Free Flight Motion of Missiles with Slight Configurational Asymmetries," Ballistic Research Laboratories Report No. 858, June 1953. AD 26405.
4. M. J. Piddington, "Deformation Characteristics of One Lot (LC SP412) of 5.56mm M-193 Ammunition," Ballistic Research Laboratories Memorandum Report No. 2016, October 1969. AD 862966.
5. J. C. McMullen, "Wind Tunnel Testing Facilities at Ballistic Research Laboratories," Ballistic Research Laboratories Memorandum Report No. 1292, July 1960. AD 244180.
6. Anders S. Platou, "Magnus Characteristics of Finned and Nonfinned Projectiles," AIAA J. 3, pp. 83-90, 1965.
7. Jack B. Carman and James C. Uselton, "Experimental Magnus Characteristics of Basic and Boattail Configurations of 3- and 5-Caliber Army-Navy Spinner Projectiles at Supersonic Mach Numbers," AEDC-TR-69-178, November 1969.
8. E. R. Benton, "Supersonic Magnus Effect on a Finned Missile," AIAA J. 2, p. 153, 1964.
9. W. F. Braun, "The Free Flight Aerodynamics Range," Ballistic Research Laboratories Report No. 1048, July 1958. AD 202249.

**UNCLASSIFIED**  
Security Classification

**DOCUMENT CONTROL DATA - R & D**

(Security classification of title, body of abstract and indexing annotation must be entered when the overall report is classified)

<b>1. ORIGINATING ACTIVITY (Corporate author)</b> U.S. Army Aberdeen Research & Development Center Ballistic Research Laboratories Aberdeen Proving Ground, Maryland 21005		<b>2a. REPORT SECURITY CLASSIFICATION</b> Unclassified	
		<b>2b. GROUP</b>	
<b>3. REPORT TITLE</b> THE INFLUENCE OF HELICAL SERRATIONS AND BULLET ENGRAVING ON THE AERODYNAMIC AND STABILITY PROPERTIES OF A BODY OF REVOLUTION WITH SPIN			
<b>4. DESCRIPTIVE NOTES (Type of report and inclusive dates)</b>			
<b>5. AUTHOR(S) (First name, middle initial, last name)</b> Maurice A. Sylvester and Walter F. Braw			
<b>6. REPORT DATE</b> November 1970		<b>7a. TOTAL NO. OF PAGES</b> 53	<b>7b. NO. OF REFS</b> 9
<b>8a. CONTRACT OR GRANT NO.</b>		<b>8b. ORIGINATOR'S REPORT NUMBER(S)</b>	
<b>a. PROJECT NO.</b> IT061102A337 (BRL) IW562604A607 (SASA)		BRL Report No. 1514	
<b>c.</b>		<b>8c. OTHER REPORT NO(S) (Any other numbers that may be assigned this report)</b>	
<b>d.</b>			
<b>10. DISTRIBUTION STATEMENT</b> This document has been approved for public release and sale; its distribution is unlimited.			
<b>11. SUPPLEMENTARY NOTES</b>		<b>12. SPONSORING MILITARY ACTIVITY</b> U. S. Army Materiel Command Washington, D. C.	
<b>13. ABSTRACT</b> Discrepancies in the predicted and observed stability behavior of bullets sometimes occur at longer ranges. Experiments in the BRL supersonic wind tunnel and range suggest that this behavior may be due to subtle aerodynamic effects of the helical engraving. The wind tunnel tests were made at supersonic Mach numbers on spinning models with accentuated helical serrations. The tests covered a range of angle of attack, Reynolds number and mismatch between the spin of the model and the twist of the serrations. The serrated model test results show yaw force and moment characteristics basically different than the Magnus results for a similar but nonserrated model. These serrated results indicate yaw forces and moments at higher angles of attack which are finite even at zero spin and which then decrease and reverse sign as the spin increases. At lower angles of attack the yaw data are extremely sensitive to the Reynolds number and the boundary layer condition and may be highly nonlinear with both angle of attack and spin mismatch.  The range data were obtained on both standard ammunition and models. For the roll damping moment a formulation is proposed and the roll moment coefficients are established for one particular model. The effects on the static moments are shown to be negligible. The Magnus and damping moments are changed, indicating a requirement for a formulation not dependent on mirror symmetry. The exponential damping coefficients show an increase in the fast mode damping with underspin and indicate strong nonlinearities in the slow mode.			

**DD FORM 1473**  
1 NOV 65

REPLACES DD FORM 1473, 1 JAN 64, WHICH IS OBSOLETE FOR ARMY USE.

**UNCLASSIFIED**  
Security Classification

14. KEY WORDS	LINK A		LINK B		LINK C	
	ROLE	WT	ROLE	WT	ROLE	WT
Aerodynamic Properties Spinning Projectiles Bullet Engraving Effects Mirror Asymmetries Serrated Models Wind Tunnel Tests Range Tests Magnus Characteristics						